

**DETECTION OF STANDING AND SITTING VARIATIONS
BASED ON IN-SOCKET PIEZOELECTRIC SENSORS FOR
TRANSFEMORAL AMPUTEES**

TAWFIK YAHYA MOHAMMED ALNUSAIRI

**FACULTY OF ENGINEERING
UNIVERSITY OF MALAYA
KUALA LUMPUR**

2020

**DETECTION OF STANDING AND SITTING
VARIATIONS BASED ON IN-SOCKET
PIEZOELECTRIC SENSORS FOR TRANSFEMORAL
AMPUTEES**

TAWFIK YAHYA MOHAMMED ALNUSAIRI

**DISSERTATION SUBMITTED IN FULFILMENT OF
THE REQUIREMENTS FOR THE DEGREE OF MASTER
OF ENGINEERING SCIENCE**

**FACULTY OF ENGINEERING
UNIVERSITY OF MALAYA
KUALA LUMPUR**

2020

UNIVERSITY OF MALAYA
ORIGINAL LITERARY WORK DECLARATION

Name of Candidate: Tawfik Yahya Al-Nusairi

Matric No: KGA 160005

Name of Degree: Master of Engineering Science

Title of Project Paper/Research Report/Dissertation/Thesis (“this Work”): Detection of Standing and Sitting Variations Based on In-Socket Piezoelectric Sensors for Transfemoral Amputees

Field of Study: Rehabilitation Engineering

I do solemnly and sincerely declare that:

- (1) I am the sole author/writer of this Work;
- (2) This Work is original;
- (3) Any use of any work in which copyright exists was done by way of fair dealing and for permitted purposes and any excerpt or extract from, or reference to or reproduction of any copyright work has been disclosed expressly and sufficiently and the title of the Work and its authorship have been acknowledged in this Work;
- (4) I do not have any actual knowledge nor do I ought reasonably to know that the making of this work constitutes an infringement of any copyright work;
- (5) I hereby assign all and every rights in the copyright to this Work to the University of Malaya (“UM”), who henceforth shall be owner of the copyright in this Work and that any reproduction or use in any form or by any means whatsoever is prohibited without the written consent of UM having been first had and obtained;
- (6) I am fully aware that if in the course of making this Work I have infringed any copyright whether intentionally or otherwise, I may be subject to legal action or any other action as may be determined by UM.

Candidate’s Signature

Date: 08/08/2020

Subscribed and solemnly declared before,

Witness’s Signature

Date:

Name:

Designation

DETECTION OF STANDING AND SITTING VARIATIONS BASED ON IN-SOCKET PIEZOELECTRIC SENSORS FOR TRANSFEMORAL AMPUTEES

ABSTRACT

A transfemoral prosthesis is required to assist amputees to perform activities of daily living (ADL). The purely mechanical or passive prosthesis has some drawbacks such as consumption of high metabolic energy and limitations in mimicking normal dynamics and kinematics of gait pattern. In contrast, the active prosthesis offers better performance and consumes less metabolic energy. However, recent active prosthesis uses surface electromyography as its sensory system which requires massive preparation work, causes sores to the patient by its electrodes and requires a lot of computation to extract meaningful features. This thesis focuses on developing signal conditioning circuitry to classify six different activities related to sit-to-stand of a transfemoral amputee using piezoelectric sensors as an in-socket sensory system. Also, it determines the optimal classifier by evaluating fifteen time-domain and frequency-domain features and selecting effective feature sets, and it investigates the effects of window size on the classification accuracy.

Fifteen piezoelectric film sensors were embedded in the inner socket wall adjacent to the most active regions of the agonist and antagonist knee extensor and flexor muscles, an i.e. region with the highest level of muscle contractions of the quadriceps and hamstring. A male transfemoral amputee wore the instrumented socket and was instructed to perform several sitting and standing variations using an armless chair. Data were collected from the fifteen sensors and went through signal conditioning circuits. The overlapped technique was used to segment the data using different window lengths. Fifteen time-domain and frequency-domain features were extracted and new feature sets were obtained based on the feature performance. Eight of the common pattern recognition

multiclass classifiers were evaluated and compared. Regression analysis was used to investigate the impact of the number of features and the window lengths on classifiers' accuracies. The classification accuracy was first calculated using k-fold cross-validation method, and 20% of data set was held out for testing the optimal classifier.

It was shown that the integration of the developed signal conditioning circuitry, the experimental protocol, and the data collection method could generate a consistent and distinguish signal pattern for each sit-to-stand and stand-to-sit related activity. The results showed that 2-feature set consisting of the root mean square (RMS) and the number of peaks achieved the highest classification accuracy with most of the classifiers. Also, it showed that varying a segment length from 150 ms to 600 ms had no significant effects on support vector machine (SVM) classifiers using the 2-feature set. SVM with cubic kernel was suggested to be the optimal classifier, and a classification accuracy of 98.33 % was achieved using the test data set.

In conclusion, this work demonstrates the use of in-socket piezoelectric sensors to classify activities of a transfemoral amputee using pattern recognition. Different variations of sitting and standing activities were accurately classified using two time-domain features and SVM with cubic kernel.

Keywords: Transfemoral amputee; transfemoral prosthesis; piezoelectric sensor; in-socket sensors; classification

**PENGESANAN VARIASI BERDIRI DAN DUDUK BERDASARKAN SENSOR
PIEZOELEKTRIK DALAM SOCKET UNTUK ORANG KURANG UPAYA
TRANSFEMORAL**

ABSTRAK

Kaki prostetik transfemoral diperlukan untuk membantu orang kurang upaya untuk menjalankan aktiviti kehidupan seharian. Kaki prostetik mekanikal atau pasif mempunyai beberapa kelemahan. Antaranya, penggunaan tenaga metabolik yang tinggi dan tidak dapat mengikut ciri-ciri dinamik dan kinematik gaya berjalan yang normal. Sebaliknya, prostesis aktif menawarkan prestasi yang lebih baik dan menggunakan tenaga metabolik yang kurang. Walau bagaimanapun, kebanyakan prostesis aktif yang terkini menggunakan elektromiografi (EMG) sebagai sistem deria yang memerlukan penyediaan yang remeh, boleh menyebabkan luka-luka kepada pesakit oleh elektrod yang digunakan dan memerlukan banyak pengiraan untuk mengekstrak ciri-ciri daripada isyarat sistem deria tersebut. Fokus tesis ini ialah pada pembikinan litar elektrik untuk menyelaras isyarat yang diperolehi daripada sistem sensori di dalam soket yang menggunakan beberapa sensor piezoelektrik bagi mengklasifikasikan enam jenis aktiviti berkaitan duduk-ke-berdiri pada orang yang kudung transfemoral. Selain itu, ia menentukan kaedah klasifikasi yang paling tepat dengan menilai ciri-ciri berasaskan domain masa yang optimum dan memilih set ciri-ciri yang berfungsi dengan baik, dan mengenal-pasti kesan saiz tettingkap pada ketepatan dalam mengklasifikasi aktiviti-aktiviti itu.

Lima belas sensor piezoelektrik diletakkan di bahagian dalam dinding soket supaya ia bersentuhan dengan kawasan paling aktif agonist dan antagonis lutut extensor dan otot flexor, iaitu kawasan yang merekodkan kadar kontraksi otot quadriceps dan hamstring yang tertinggi. Seorang subjek lelaki yang diamputasi tahap transfemoral memakai soket yang dipasangkan dengan sensor itu dan diarahkan untuk melakukan beberapa variasi pergerakan duduk dan berdiri menggunakan kerusi tanpa pemegang. Data dikumpulkan

dari lima belas sensor dan melalui litar penyaman isyarat. Teknik bertindih digunakan untuk menyusun data menggunakan tetingkap yang berbeza kepanjangan. Tiga belas ciri-ciri berasaskan domain masa telah diekstrak dan set ciri-ciri baru diperolehi berdasarkan prestasi ciri. Lapan daripada klasifier yang biasa digunakan untuk mengenal pasti corak dinilai dan dibandingkan. Analisis regresi digunakan untuk mengenalpasti impak kepada ketepatan pengelas dengan perubahan bilangan ciri dan panjang tetingkap. Kaedah pengesahan bersilang '*k-fold*' digunakan untuk mengira ketepatan klasifikasi, dan 20% daripada data diasingkan untuk menilai pengelas yang optimum.

Dapat dilihat bahawa litar penyelarasan isyarat yang telah dibina, protokol eksperimen dan kaedah mengumpul data yang digunakan mampu menghasilkan isyarat yang konsisten dan mampu mengklasifikasikan setiap aktiviti antara satu sama lain. Hasil kajian menunjukkan bahawa set 2 ciri yang terdiri daripada '*Root Mean Square*' (RMS) dan bilangan puncak mencapai ketepatan klasifikasi tertinggi (97.82%) menggunakan '*Support Vector Machine*' (SVM) dengan kernel kubik. Selain itu, ia menunjukkan bahawa panjang segmen yang berbeza dari 150 ms hingga 600 ms tidak mempunyai kesan yang ketara ke atas ketepatan pengelasan menggunakan set yang terdiri daripada 2 ciri.

Keputusan menunjukkan bahawa set yang mengandungi 2-ciri yang terdiri daripada RMS dan bilangan puncak menghasilkan ketepatan klasifikasi yang tertinggi apabila diuji dengan kebanyakan pengelas. Selain itu, ia juga menunjukkan bahawa panjang segmen yang berbeza dari 150 ms hingga 600 ms tidak mempunyai kesan ketara pada SVM menggunakan set 2-ciri. SVM dengan kernel kubik dicadangkan untuk menjadi pengelas optimum dan hasil ujian dengan set data ujian mencapai ketepatan pengelasan 98.33%.

Kesimpulannya, kajian ini menunjukkan penggunaan sensor piezoelektrik dalam-soket untuk mengklasifikasikan aktiviti-aktiviti orang kurang upaya transfemoral menggunakan pengenalan corak. Berbagai variasi aktiviti duduk dan berdiri dapat

diklasifikasikan dengan tepat menggunakan dua ciri domain waktu dan SVM dengan kernel kubik.

kata kunci: Orang kurang upaya pransfemoral; prostetik transfemoral; penderia piezoelektrik; penderia di dalam soket; pengelasan

University of Malaya

ACKNOWLEDGEMENTS

All praises and glory be to Allah. I thank the almighty for giving me the courage and strength to complete this dissertation.

I would like to express my gratitude to my supervisor Dr. Nur Azah Binti Hamzaid for introducing me to the topic, guiding me throughout my master program and being patience in supervising me. She was a great mentor during my program. Also, I would like to thank Dr.Sadeeq Ali for his support and guidance to improve this work. I wish to thank members of mySmartLeg team, Dr.Farahiyah, Hanie, and Hidayah for their help and support.

I would like to thank my father and mother for their encouragement and support throughout my journey. Special thanks to my wife and my son for their patience, tolerance, and endless support.

I would like to thank my friend Tarig Almehmadi for introducing me to Dr.Nur Azah and helping me in my journey. Also, I would like to thank Waleed, Abona and Mona for their help in proof reading my publications. Special thanks for Awad Ali for printing and submitting my thesis.

University of Malaysia

TABLE OF CONTENTS

Abstract	iii
Abstrak	v
Acknowledgements	viii
Table of Contents	ix
List of Figures	xiii
List of Tables.....	xvi
List of Symbols and Abbreviations.....	xvii
List of Appendices	xviii
CHAPTER 1: INTRODUCTION.....	1
1.1 Overview.....	1
1.2 Importance of sitting and standing movements	2
1.3 Types of transfemoral prostheses	2
1.4 Sensors technology used in active transfemoral prosthesis.....	3
1.5 Piezoelectric transducers in transfemoral prostheses	5
1.6 Motivation of the study.....	6
1.7 Scope and aim of the study.....	9
1.8 Thesis structure	10
CHAPTER 2: LITERATURE REVIEW.....	11
2.1 Introduction.....	11
2.2 Passive prosthetic leg.....	11
2.3 Active prosthetic leg	14
2.4 Sitting and standing activities.....	16
2.5 Biomechanics of sit-to-stand and stand-to-sit.....	17

2.6	Sensors used in transfemoral prosthetic leg.....	18
2.7	Piezoelectric transducers	23
2.8	Pattern recognition in prosthetic limbs	27
2.8.1	Data windowing.....	28
2.8.2	Feature extraction	30
2.8.2.1	Mean Value	32
2.8.2.2	Standard deviation.....	32
2.8.2.3	Skewness	33
2.8.2.4	Variance	33
2.8.2.5	Zero crossing.....	34
2.8.2.6	Root mean square	34
2.8.2.7	Number of peaks	34
2.8.2.8	Kurtosis	35
2.8.2.9	Integral of absolute value	35
2.8.2.10	Simple square integral.....	36
2.8.2.11	Mean absolute value.....	36
2.8.2.12	Slope sign change.....	36
2.8.2.13	Mean Frequency	37
2.8.2.14	Median Frequency.....	37
2.8.2.15	Spectral power magnitude.....	38
2.8.3	Classification algorithms.....	38
2.9	Summary.....	42
CHAPTER 3: METHODOLOGY.....		45
3.1	Introduction.....	45
3.2	Materials	45

3.3	Sensors configuration and placement	46
3.4	Signal conditioning circuitry	48
3.5	Data collection	51
3.6	Experiment setup	54
3.6.1	Experimental protocol	54
3.7	Data windowing and feature selection.....	57
3.8	Pattern recognition algorithms.....	60
3.8.1	Linear discriminant analysis.....	60
3.8.2	Decision tree.....	61
3.8.3	k-Nearest-Neighbor	61
3.8.4	Artificial neural network	62
3.8.5	Support Vector Machine.....	63
3.9	Evaluation.....	64
 CHAPTER 4: RESULTS AND DISCUSSION.....		65
4.1	Data preprocessing and collection	65
4.2	Feature selection results.....	69
4.3	Effects of varying window length.....	83
4.4	Optimal classifier.....	84
4.5	Summary.....	87
 CHAPTER 5: CONCLUSION.....		89
5.1	Summary of the findings	89
5.2	Limitations of the study	91
5.3	Recommendations for future work	92
	References	93

List of Publications and Papers Presented	99
Appendix A: Approval letter from medical ethics committee	100
Appendix B: Award	101

University of Malaya

LIST OF FIGURES

Figure 1.1: Categories of the transfemoral prosthetic leg systems	3
Figure 2.1: An example of single and polycentric prosthetic knee joint (a) Otto Bock 3R95 single axis knee (ottobock, 2016b), (b) ÖSSUR Total Knee® 1900 polycentric knee(OrtoPed, 2011)	12
Figure 2.2: (a) The manual locking knee attached to a socket (PnOCare, 2012), (b) The weight-activated stance-control knee, 3R49 Otto Bock(Ottobock, 2017).....	13
Figure 2.3: Examples of non-powered active prostheses (a) C-Leg (Ottobock, 2016a), (b) Rheo Knee (Össur, 2018).....	15
Figure 2.4: Examples of powered prosthetic legs (a) the powered clutchable series-elastic knee prosthesis (Rouse et al., 2014), (b) Vanderbilt Leg (Vanderbilt, 2013).....	16
Figure 2.5: Stages of sit-to-stand movement (Yoshioka et al., 2009b).....	18
Figure 2.6: The above knee prosthesis (AKP) at different knee flexion angles (Kapti & Yucenur, 2006).....	19
Figure 2.7: Electromyographic (EMG) and Mechanical Sensor (Hargrove et al., 2015)22	
Figure 2.8: Locations of FSRs attached to the socket's wall(El-Sayed, 2015).....	25
Figure 2.9: Locations of piezo sensors inside the socket at anterior and posterior sites (El-Sayed, 2015).....	25
Figure 2.10: Flexible printed circuit board integrated with piezoelectric sensors to measure the stress between the socket's wall and the residual limb of the amputee (Maurizio et al., 2017).....	27
Figure 2.11: The overlapping method for segmenting data (Smith et al., 2011).....	29
Figure 2.12:The disjoint method for segmenting data (Oskoei & Hu, 2008)	29
Figure 2.13: Block diagram of piezo signal classification based on pattern recognition	30
Figure 3.1: Piezo Film sensor (FDT series, Measurement Specialties Product Guide)..	45
Figure 3.2: The fabricated socket equipped with the in-socket piezoelectric sensors attached to the hydraulic knee joint and the foot solid ankle cushion heel foot	46
Figure 3.3: The fifteen piezoelectric sensors placed in zigzag orientation on the socket's wall with the added elastic foundation.....	47

Figure 3.4: An active low-pass filter circuit schematic for the first anterior sensor (A1)	48
Figure 3.5: The PCB layout of the first anterior sensor (A1)	49
Figure 3.6: The signal condition circuit designed for the eight anterior sensors consisting of eight active low-pass filters	50
Figure 3.7: The signal condition circuit designed for the seven posterior sensors consisting of seven active low-pass filters	50
Figure 3.8: LabVIEW virtual instrument of the two data acquisition cards, 15 sensors, one trigger and pass-band filtered	51
Figure 3.9: A transfemoral amputee donning the in-socket based piezoelectric sensory system and the data acquisition cards connected to the signal conditioning circuits	52
Figure 3.10: The Graphical User Interface (GUI) of VICON Nexus software (Version 1.8.5) used to collect data from the two force plates	53
Figure 3.11: Trigger sensor to synchronize LabVIEW and VICON Nexus	54
Figure 3.12: Illustration of the activities performed by the subject: (a) Sit-to-stand, (b) stand-to-sit, (c) dynamic sitting, (d) static sitting, (e) dynamic standing and (f) static standing	56
Figure 3.13: The flowchart of the pattern recognition technique	58
Figure 3.14: Architecture of ANN used to classify six activities using one feature and a window of 300 size	63
Figure 4.1: Three trials of P1 and A1 signals of sit-to-stand movements with the corresponding GRFs	65
Figure 4.2: Three trials of P1 and A1 signals of stand-to-sit movements with the corresponding GRFs	66
Figure 4.3: The fifteen sensors' filtered and amplified signals of the six different activities (a) the anterior sensors, (b)Posterior sensors	67
Figure 4.4: Averaged classification errors and standard deviations of Mean and MAV features and their standard deviations with the eight classifiers	69
Figure 4.5: Classification errors and standard deviations of IAV and SSI features with the eight classifiers	70

Figure 4.6: Averaged classification errors and standard deviations of Skewness and kurtosis features with the eight classifiers	71
Figure 4.7: Averaged classification errors and standard deviations of RMS, SD, and VAR features with the eight classifiers	72
Figure 4.8: Averaged classification errors and standard deviations of Peak, ZC and SSC features with the eight classifiers	73
Figure 4.9: Averaged classification errors and standard deviations of MNF, MDF, and SPM features with the eight classifiers	74
Figure 4.10: Averaged computation time of the single features in descending order.....	77
Figure 4.11: Averaged training time of the eight test classifiers	77
Figure 4.12: The averaged computation time of the obtained five feature sets	79
Figure 4.13: Classification accuracy of the eight classifiers with the five obtained feature sets.....	80
Figure 4.14: The classification accuracies with different. Window sizes (from 150ms to 600 ms).....	83
Figure 4.15: Medians and confidence interval accuracies of SVM with cubic kernel ...	85

LIST OF TABLES

Table 2.1: Summary of the state-of-the-art literature review on the pattern recognition technique with prosthetic applications	40
Table 3.1: Experiment protocol of activities.....	57
Table 4.1: Classification accuracy (%) of the 15 single features with the eight classifiers	75
Table 4.2: Descriptive statistics (mean, standard deviation, minimum and maximum) of features' computation time.....	76
Table 4.3: Prediction time of the classifiers.....	78
Table 4.4: The relationship between increasing the number of features and the classification accuracy	82
Table 4.5: <i>P-values</i> of a regression analysis to investigate the impact of window lengths on classifiers' classification accuracies.....	84
Table 4.6: Confusion matrix of the testing data set classified by SVM with cubic kernel	86

LIST OF SYMBOLS AND ABBREVIATIONS

ADL	:	Activity of daily living
GRF	:	Ground reaction force
EMG	:	electromyography
AKP	:	Above-knee prosthesis
IMU	:	Inertial Measurement Unit
FSR	:	Force sensing resistor
EEG	:	Electroencephalography
CA	:	Cushion-All
SVM	:	Support vector machine
ANN	:	Artificial neural network
LDA	:	Linear discriminant analysis
DT	:	Decision tree
k-NN	:	k-nearest neighbors
MNF	:	Mean frequency
MDF	:	Median frequency
SPM	:	Spectral power magnitudes

LIST OF APPENDICES

APPENDIX A: APPROVAL LETTER FROM MEDICAL ETHICS COMMITTEE	85
APPENDIX B: AWARD	86

University of Malaya

CHAPTER 1: INTRODUCTION

1.1 Overview

The term disability, in many cases, is commonly attributed to limitations in normal human movement, vision, respiration, hearing, or balance. It can be highlighted that both disabled and nondisabled people have the same health needs that enable them to practice the activities of daily living such as feeding and oneself, work, and other activities. Movement-related disabilities are either congenital (birth defects) or occur during someone's life (El-Sayed et al., 2015). The former is present from birth whereas the latter emerges in some people after particular diseases or accidents during their lifetime which, as a result, leads to upper or lower extremities amputations. In some cases, additional assistive devices are required to help them perform these activities. Limitations in movements, especially for people with major lower limb amputations, restrict their performance of basic daily activities such as walking, stair ascent/descent, running, standing and sitting (El-Sayed et al., 2015).

Amputees confront emotional and financial changes due to the tragic loss of their limbs. Amputees require assistive devices to replace the missing limb(s). Prosthetic legs are artificial devices that replace the missing parts of a leg and restore functions of a sound leg. Prosthetic legs can be categorized into two groups (transtibial prosthesis and transfemoral prosthesis). The first category (transtibial prosthesis) is an artificial device that replaces the missing part of a leg amputated below the knee joint. The second category (transfemoral prosthesis) is an artificial limb which replaces above-knee amputated legs (Brooker, 2012).

1.2 Importance of sitting and standing movements

Standing from seating position or a chair to upright posture is called sit-to-stand while sitting from standing position is called stand-to-sit. These two movements are two of the most essential and common daily activities. According to Yoshioka et al., (2009), sit-to-stand and stand-to-sit are performed at least 120 times per day which means each movement is repeated 60 times. These movements are considered pre-requisites and post-requisites for upright movements such as walking, stair ascending and descending, and ramp walking. Also, performing these activities ensures the amputee's independence. For instance, if amputees require someone to help and support them whenever they perform these movements, this will cause a burden on the caretaker. Therefore, performing these movements independently is a fundamental component for independence (Demura & Yamada, 2007). Additionally, in the mechanical term, sit-to-stand and stand-to-sit are considered among the most demanding activities. Sit-to-stand, for instance, requires a greater peak joint moment compared to other movements (walking or stair ascending). Three joints are mainly involved in performing sit-to-stand and stand-to-sit, namely, hip, knee, and ankle joints. A transtibial amputee can perform these activities easier than a transfemoral amputee. A transfemoral amputee lacks two joints (knee and ankle) while a transtibial amputee lacks only one joint (ankle).

1.3 Types of transfemoral prostheses

There are two major categories of transfemoral prostheses, passive (purely mechanical) and active (computerized). The passive type has pre-programable movements that replicate the movements of the sound leg, and it has a mechanical structure and requires no power source to operate. Although the passive prosthesis is the most durable and the most economical among the available prostheses, it is less adaptive to environment's disturbances

compared to active prostheses (Martinez-Vilialpando & Herr, 2009). Moreover, the passive prosthetic legs can be classified based on the number of knee axes (single axis or multi-axis), fluid control system (pneumatic and hydraulic), and locking system (manual and weight-activated) (Wang et al., 2005). On the other hand, the active type is equipped with an adaptive controller and actuator/s in the knee joint (Popovic et al., 1991). The active prostheses can be categorized based on the actuator type (powered knee or non-powered knee) which generates torque during activities. Figure 1.1 depicts the classification of the transfemoral prosthetic leg systems.

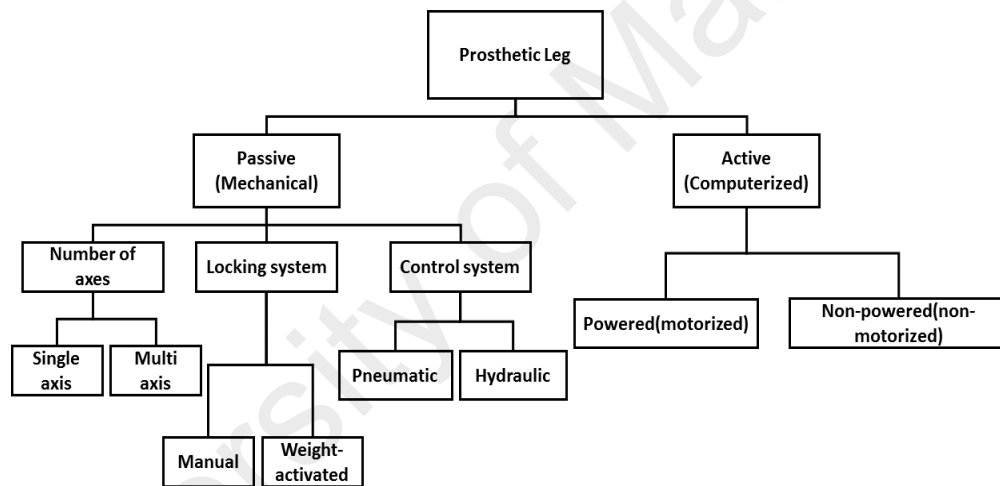


Figure 1.1: Categories of the transfemoral prosthetic leg systems

1.4 Sensors technology used in active transfemoral prosthesis

The active prosthesis could cope with most of the passive prosthesis limitations with the help of embedded sensors, controllers and actuators (Jasni et al., 2016). Mainly, there are two

approaches to control the active prosthetic leg which can be classified as follow: 1) approach uses dynamic mechanical sensors which interact between the user and the residual limb, 2) approach measures muscle electrical activities in the residual limb using surface electromyography (SEMG) (Dawley et al., 2013; Yuan et al., 2015). The first approach is used by most of the active prosthetic legs, currently in use, that has sensory systems located away from muscles and knee axis. These mechanical sensory systems measure different parameters such as position, force, velocity, phase transitions, and torque to improve the controllability of the prosthesis. Parameters identification is essential to control the prosthesis by detecting the current or intended user's movements (El-Sayed, Hamzaid, & Abu Osman, 2014b).

On the other hand, sensors closer to the muscles and knee axis can yield more accurate parameters which can be used to derive the user's state of movement instantaneously. The second approach (EMG-based) was first introduced in 1991 to control a multifunction prosthesis (B. Hudgins et al., 1991). The EMG-based approach uses electrodes to detect the electrical activity produced by muscle, and then the acquired signal is fed to the controller. Previous work focused on using EMG measured signal as an input to a pattern recognition architecture and control the prosthetic by predetermined states (Huang, Kuiken, & Lipschutz, 2009). However, EMG technique has some drawbacks. Massive preparation work is needed to accurately place the electrodes in their proper positions which causes discomfort and skin problem to the user. Additionally, electrodes could cause sores for the patient because of movements between the amputee's residual limb and the socket's wall (Hargrove et al., 2013). Feature extraction of the EMG signal is computationally intensive (Li et al., 2012).

1.5 Piezoelectric transducers in transfemoral prostheses

Smart or intelligent materials can be found in several forms such as piezoelectric materials, magnetorheological fluids, and shape memory alloy, which are used in industrial, surgical and medical applications. They have the ability to respond to external stimuli such as temperature or stress. Smart materials' properties allow smart materials to simulate or respond to environmental changes (El-Sayed et al., 2013). Piezoelectric materials have the ability to act as sensors or actuators. For instance, if a mechanical stress is applied on piezoelectric materials, electric charges will be generated. These electric charges will be proportional to the mechanical stress applied and are measured in volts. On the other hand, if electric charges are applied on piezoelectric materials, piezoelectric materials will contract and expand based on the polarity direction.

Due to the ability of piezoelectric materials to act as sensors, researchers have attempted to utilize them in measuring the pressure between the socket and residual limb in the lower amputation field. A feasibility study, for instance, was conducted to identify prosthetic knee movements via pattern recognition of mechanical responses of force sensing resistor (FSR) and piezoelectric sensors (in two different setups) attached to the socket's wall of a prosthesis (El-Sayed et al., 2015). The study showed that piezoelectric sensors could identify a wide range of measurements including phases of different movements such as mid swing and terminal swing, pre-full standing and stair ascent. On the other hand, FSR has some measurement limitations and could only estimate the gait cycle stance, and at the sit-to-stand movement, it could only estimate the pre-full standing phase. Furthermore, in another efficacy study (Jasni et al., 2016), a sensory system that uses piezo transducers inside a prosthetic socket was developed. The piezo transducers were placed in direct contact with

the remaining part of the amputee's leg (residual limb). In addition, the piezoelectric sensors were positioned in a zigzag orientation in order to cover the active regions of the two major muscle groups of the upper leg (Hamstrings and Quadriceps), and the proposed design showed its effectiveness for a transfemoral prosthesis.

1.6 Motivation of the study

Safely performing ADL, such as sitting down on a chair or standing up, is an essential element in ensuring independent functioning (Zijlstra et al., 2012). Conversely, confronting difficulties in performing these movements, which are prerequisites for gait and upright mobility, lead to a sedentary lifestyle (Kralj et al., 1990; Zijlstra et al., 2012). In comparison to non-amputees, transfemoral amputees utilize more metabolic energy (60% higher) and apply greater torque and power (300% higher) on the amputated side of their bodies (Jasni et al., 2016; Wang et al., 2013).

Passive and active prostheses are used to assist amputees to perform ADL. The passive type has pre-programmable movements that replicate the movements of the sound leg (Grimmer & Seyfarth, 2014; Popovic et al., 1991) while the active type is equipped with an adaptive controller and actuator/s in the knee joint (Popovic et al., 1991). Although the current passive prostheses improve the quality of life of transfemoral amputees (Chen et al., 2013), these passive prostheses do not adequately fulfill the needs of amputees during sitting down and standing up owing to the lack of external power which assists the elevation of the body weight and the high consumption of metabolic energy (Kapti & Yucenur, 2006; Lara-Barrios et al., 2018). Powered active prostheses were introduced to overcome these shortcomings with the help of embedded electronics, controllers and electromechanical actuators (Huang et al., 2011; Jasni et al., 2016). Most of the active prosthetic legs, currently

in use, have embedded sensory systems located away from muscles which measure different parameters such as position, force, velocity, phase transitions, and torque to control a prosthesis system (El-Sayed et al., 2015). Inertial Measurement Units were utilized by Mueller, Evans (2011) to obtain kinetic and kinematic data of lower limb prostheses. On the other hand, other active prosthetic legs utilize sensors closer to the muscles that provide information about neuromuscular activities which can be used to derive the user's state of movement instantaneously (EMG-based approach) (El-Sayed et al., 2015; Huang et al., 2005). However, the EMG technique has some drawbacks such as the necessity for skin preparation (shaving and applying gel before donning the socket) and weak signals with microvolt-level intensity which requires complex amplification circuitry. Also, EMG requires a relatively high number of electrodes which results in computationally intensive feature extraction (Li et al., 2012). For instance, in a study conducted by Hargrove et al. (2013), a grid of 96 electrodes and 13 mechanical sensors were used to classify movements of a transfemoral amputee. Extracting features from 109 sensors would be computationally expensive for the processor and would lead to a lag in the system's response, therefore, which would make the controller unable to function in real-time. Moreover, the classification of EMG signals requires extracting a high number of frequency-domain and time-domain features. For instance, Geethanjali & Ray (2014) used a feature set consisting of 32 features extracted from EMG electrodes and linear discriminate analysis classifier to classify six movements of two transradial amputees. This high number of extracted features would put extra load on the processor.

To find an alternative for the EMG technique, researchers have attempted to measure the pressure between a socket and a stump of an amputee. For instance, the pressure of the transfemoral amputee's stump (forces applied to the x-direction) was measured using Flexiforce network sensors which consisted of five embedded force sensors attached to the socket's wall (El-Sayed et al., 2014). MEMS-based bubble pressure sensor and custom electronics were used to acquire interface pressure between a socket and an amputee's stump (Wheeler et al., 2011). Moreover, piezoelectric materials were utilized to measure the pressure between the socket and residual limb in the lower amputation field due to the ability of acting as sensors. In a study conducted by Maurizio et al. (2017), piezoelectric sensors were utilized to measure normal pressure (both dynamic and static) in order to monitor the stress caused by the contact between prosthesis' wall and the residual limb of an amputee. Additionally, Lorenzelli, Sordo (2017) developed a tri-axial force piezoelectric sensor which maps interaction forces between a socket and a leg of a transfemoral amputee. A feasibility study was conducted by El-Sayed, Hamzaid (2015) to identify prosthetic knee movements via pattern recognition of responses of piezoelectric sensors attached to the socket's wall of a prosthesis. Findings from the study showed that piezoelectric sensors could identify a wide range of measurements including phases of different movements such as mid swing and terminal swing, pre-full standing and stair ascent.

Utilizing piezoelectric sensors as a sensory system of a prosthetic leg would eliminate the preparation work before donning the socket and would require relatively simpler circuitry to filter and amplify sensors' signals compared to EMG. Also, the thickness of the piezoelectric sensors could be less than 0.03 mm which makes suitable to be placed on the internal wall of a socket and caused less skin impingement compared to EMG electrodes since the thickness

of EMG electrodes ranges from (5 mm to 15mm) (Hefferman et al., 2015). However, transfemoral amputees have substantial differences in the length of their stumps and very high variation ratios of muscles' activities during locomotion (including hamstring and quadriceps) which affect the placement of the piezoelectric sensors and makes it impossible to standardize sensors configurations and placement (Wu et al., 2004)8/10/20 10:52:00 PM.

Controlling active prosthesis based on information gathered from the residual limb is still at an experimental level apart from few commercially available technologies that use mechanical-based sensors to derive the residual limb movement. Moreover, the piezoelectric sensory system is still in its first stage and more work is required to develop and validate it. To date, no previous studies have been done to classify sitting and standing movements using piezoelectric sensors. Therefore, this thesis investigates if the piezoelectric sensor is a good alternative to control the powered prostheses by developing a proper method to classify variations of sitting and standing activities using the pattern recognition technique.

1.7 Scope and aim of the study

Improving the control system of the prosthesis requires a better sensory system and more information from the user's states to enhance the prosthesis performance. This study aims to develop signal conditioning circuitry for in-socket piezoelectric sensors to collect and preprocess data which requires studying the characteristics and properties of the sensors, knowledge about digital signal processing, and data acquisition devices. After preprocessing the data, multiclass classifiers would classify six different activities of a transfemoral amputee which needs comprehensive knowledge and experience of data segmentation, feature extraction, feature selection, programming, statistics, classification algorithms, and machine learning techniques. The specific objectives of the study can be listed as follows:

1. To generate a consistent and distinguish signal pattern for each sitting and standing variations by developing signal conditioning circuitry for the in-socket sensory system, a data collection method, and an experimental protocol.
2. To identify the most effective feature set and investigate the effects of varying window lengths on the classification accuracy.
3. To determine the optimal classifier for categorizing six variations of sitting and standing activities of a transfemoral amputee via in-socket sensory system utilizing piezoelectric-based in socket sensors.

1.8 Thesis structure

This thesis has five chapters. The first chapter presents the introduction, research motivation and the aim of the study. The second chapter contains the literature review which depicts the current technologies used in the prosthetic leg field. The third chapter demonstrates the methodology used in this thesis, experiment setup, data collection, feature selection, and pattern recognition algorithms. The fourth chapter illustrates the experiment's results and discusses the impacts of the results. The last chapter is the conclusion which sums up the whole thesis, gives recommendations and highlights the limitations of the thesis.

CHAPTER 2: LITERATURE REVIEW

2.1 Introduction

The development in the field of transfemoral prosthetic leg helps amputees to perform daily life activities in a normal way like non-disable people. For this reason, researchers have been encouraged to develop and improve the technology used in transfemoral prostheses and the sensory system of the prostheses is no exception.

This chapter depicts the latest technology advancements in the field of the transfemoral prosthesis. Different types of sensory systems used in transfemoral prostheses development and their functionalities are discussed. Also, the biomechanics and phases of sit-to-stand and stand-to-sit movements are presented. Most popular pattern recognition classification algorithms are presented as well. Furthermore, data windowing methods and feature extraction are reviewed in this chapter.

2.2 Passive prosthetic leg

The single axis knee has only one axis of rotation which allows it to swing backward and forward like a door hinge. It is considered the most economical knee and most durable. Therefore, it is used mostly by children since they grow up quickly and need to replace the prostheses when they get older. The single-axis prosthesis has several limitations. It has no stance control, also; it is free-swinging. Amputees need to use their muscles to stabilize and control the prosthesis. In contrast, the polycentric (multi-axis) knee, is also called the four-bar knee, has more than one axis of rotation which offers more stability during the stance phase. Also, it can be bent easily during the swing phase. Examples of the single axis and multi-axis prostheses are shown in Figure 2.1 (Grant McGimpsey & Terry C. Bradford, 2011).



(a)



(b)

Figure 2.1: An example of single and polycentric prosthetic knee joint (a) Otto Bock 3R95 single axis knee (ottobock, 2016b), (b) ÖSSUR Total Knee® 1900 polycentric knee(OrtoPed, 2011)

The passive prosthetic leg uses fluid dynamic (pneumatic and hydraulic) systems to provide fixed impedance, and the friction of the prosthesis varies based on the speed of the walking amputee. The pneumatic system stores energy during knee flexion (compressing air) and releases energy via knee extension. The hydraulic system can provide a wider range of walking speed compared to the pneumatic system. Instead of air, the hydraulic system uses silicone oil which provides smoother gait. Although the hydraulic offers performances close to the normal of the sound knee, costs more, requires more maintenances, and weights more compared to the pneumatic system (El-Sayed et al., 2014).

The passive prosthetic legs have no sensors to ease the interaction between amputees and the environment. There are two approaches to stabilize the prosthesis during stance phase; manual locking and the weight-activated stance-control. The manual locking approach which the amputee walks with a stiff knee utilizes a lever to unlock the knee in order to stabilize the user during knee extension, as shown in Figure 2.2(a) This prosthesis requires

high energy during walking which the amputee has to bear (Jay Martin, 2010). Another approach is the weight-activated stance-control knee, shown in Figure 2.2(b), which can be found in both single axis and polycentric knee. It uses a constant friction to stabilize the prosthesis during the stance phase. When the weight of the body transfers to the prosthesis, an embedded brake will be activated to prevent buckling (Martinez-Vilialpando & Herr, 2009). A spring, which can store energy, is used to aid the prosthesis during the swing phase by loading during weight bearing and releasing the energy stored during the swing phase. One drawback is that it requires accurate and frequent adjustments to ensure the lock is working effectively. Also, only one walking speed can be set to this kind of prosthesis. However, most of the recent polycentric prostheses use either hydraulic or pneumatic swing control to adjust the walking speed.



(a)



(b)

Figure 2.2: (a) The manual locking knee attached to a socket (PnOCare, 2012), (b) The weight-activated stance-control knee, 3R49 Otto Bock (Ottobock, 2017)

Generally, the passive prosthesis is used in the prosthetic limb field due to its robustness, light weight, and low cost. Nevertheless, amputees need to stabilize the prosthesis during standing using their muscles which might cause fatigue. Additionally, in comparison to non-amputees, transfemoral amputees with non-powered prostheses utilize more metabolic energy (60% higher) and apply greater torque and power (300% higher) on the amputated side of their bodies (Jasni et al., 2016; Waters RL et al., 1976).

2.3 Active prosthetic leg

Due to the advancements in technology and the need to overcome passive prosthesis drawbacks, the passive prosthetic leg was upgraded to the active prosthetic leg which equipped with microprocessor and sensors to control the actuators in order to increase the flexibility and knee angle range during movement. Sensors' main function in the active prosthetic leg is to measure the parameters of the leg's kinematic (knee angle) and kinetic (torque). The active prosthetic leg can be grouped into powered (motorized) prosthesis and non-powered prosthesis.

The active non-powered prosthesis, also called adaptive dissipative prosthesis, utilizes a microprocessor, sensors, and actuators to adjust the impedance. A microprocessor is used to regulate the impedance by tuning fluid dynamics. For instance, the microprocessor in C-leg (manufactured by Otto Bock) tunes hydraulic values to adjust the impedance, and in Rheo knee (manufactured by Össur), it controls the impedance by varying the magnetic field in a magnetorheological fluid. However, this type of prosthetic legs cannot support the amputee to perform energy-demand activities such as stair climbing and sit-to-stand. Figure 2.3 shows two examples of active prosthetic legs (the Rheo Knee and the C-leg).



(a)



(b)

Figure 2.3: Examples of non-powered active prostheses (a) C-Leg (Ottobock, 2016a), (b) Rheo Knee (Össur, 2018)

The powered or motorized prosthetic leg is another type of the active prosthesis which has the capability to support and assist an amputee to perform several activities such as ramp descent, standing, stair descent, and level walking. Furthermore, the powered prosthetic leg has the ability to detect instances of stumble (Jay Martin, 2010). Moreover, having external power enables the prosthesis to adapt to walking in different environments. Although powered prosthetic leg assists amputees to perform the mentioned motions, it has some limitations when it comes to delivering sufficient joint power to perform movements such as sit-to-stand movement and stair climbing (Wolf et al., 2012). Example of the powered prostheses are the active agonist-antagonist knee prosthesis (Martinez-Vilalpando & Herr, 2009), the powered clutchable series-elastic knee prosthesis (Rouse, Mooney, & Herr, 2014),

Össur Powered Knee, and the Vanderbilt leg (Sup et al., 2009). Figure 2.4 illustrates examples of powered artificial legs.

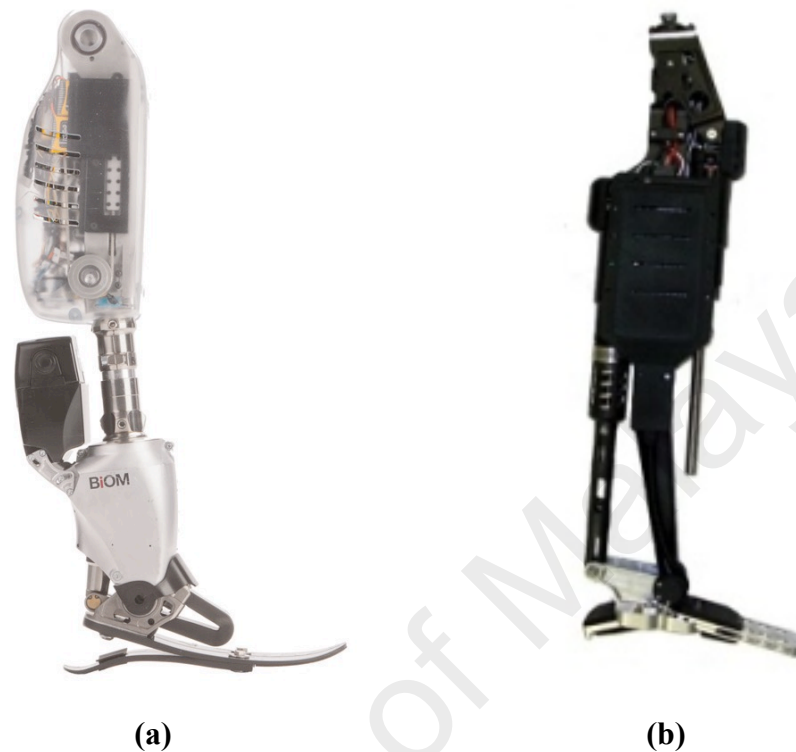


Figure 2.4: Examples of powered prosthetic legs (a) the powered clutchable series-elastic knee prosthesis (Rouse et al., 2014), (b) Vanderbilt Leg (Vanderbilt, 2013)

2.4 Sitting and standing activities

Safely performing daily life activities, such as sitting down on a chair or standing up, is essential in ensuring independent functioning. On the other hand, confronting difficulties in performing such movements lead to an inactive lifestyle (Zijlstra et al., 2012). Thus, movements such as sitting and standing up are vital to amputees and prerequisites for gait and upright mobility. Besides, standing up is essential for several organs to function properly such as bladder, kidney, and intestines. Moreover, standing up helps in maintaining proper bone shape (Kralj, Jaeger, & Munih, 1990). Walking, stair ascending and descending are examples of everyday activities performed while standing. Inabilities or difficulties in

performing these movements easily lead to falling. Many studies have been conducted to measure, analyze and detect sitting and standing movements to avoid the risk of falling. Falling can cause major injuries for amputees and can negatively change their self-confidence. However, most of these studies were conducted on healthy and elderly subjects, not on transfemoral amputees. For instance, in one study (Wheeler et al., 1985) healthy adult women subjects were recruited to perform sit-to-stand movements, and video cameras, EMG electrodes (positioned on vastus lateralis and triceps brachii), force plates, and seat switches were utilized to measure and analyze the movement. In other studies, accelerometer, optoelectronic system and gyroscope were utilized. Several determinants were considered in these studies such as the height of a chair, the arm position, the speed of performing the movement, and the foot and knee positions. Some studies divided the sit-to-stand and stand-to-sit into five phases, others into only two phases while the majority divided them into three phases (Galli et al., 2000; Hesse et al., 1994; Park et al., 2003).

2.5 Biomechanics of sit-to-stand and stand-to-sit

Standing up from a chair to an upright posture while maintaining balance is defined as a sit-to-stand movement, which is considered one of the frequent daily activities. Sit-to-stand movement can be divided into three phases, as shown in Figure 2.5; 1) Start (Sitting Posture Phase), when an individual starts moving from a sitting posture; 2) Seat-off (Sit-to-Stand transfer Phase), when the individual's bottom leaves the chair; 3) Finish (Standing Phase), when the individual is in a fully upright posture (Yoshioka et al., 2009). The first phase starts by tilting the anterior pelvic which gives rising's initial momentum followed by a trunk extension and hip flexion and ends before the glutes leave the chair. The second phase starts after the ankles reach their maximum dorsiflexion. The hamstrings muscles group supports

the body during the transition by flexing the knee joint and extending the thigh. Glutes are responsible for straightening out hips, and this phase ends when the hips stop extending. The last phase is standing which requires calf muscle, soleus and gastrocnemius to stabilize the body during standing (Kotake T et al., 1993; Roebroek et al., 1994).

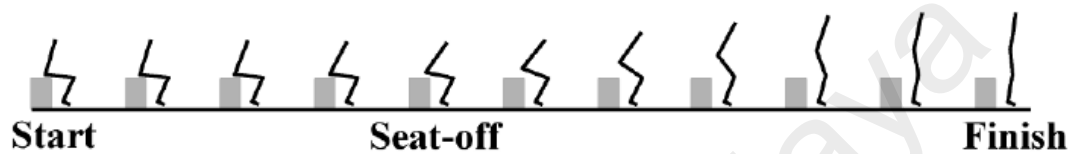


Figure 2.5: Stages of sit-to-stand movement (Yoshioka et al., 2009b)

Sitting down from upright postures is defined as a stand-to-sit movement. It is vital for physical independence and one of the basic movements in daily mobility. Like sit-to-stand, stand-to-sit movement can also be divided into three phases; 1) Start (Standing Phase), when an individual is in an upright posture and start preparing to sit down; 2) Seat-on (Stand-to-Sit Transfer Phase), when the individual's bottom starts touching the chair; 3) Finish (Sitting Phase), when the individual is in sitting position (Tsukahara et al., 2010).

2.6 Sensors used in transfemoral prosthetic leg

In order for a prosthetic leg to perform optimally, its control system requires several input variables; therefore, a variety of sensors is used in the prosthesis (Syrseloudis et al., 2008). The control variables need to be determined in order to select the appropriate sensory system for the prosthesis. For instance, two variables (force and flexion parameter) are required in adaptive-control of a prosthetic leg (Herr & Wilkenfeld, 2003). During a gait cycle, the

microprocessor varies the resistance of the knee joint according to the acquired information from the sensors. In addition, the knee flexion/ extension was measured by angle sensors that were attached to the knee axis. A study conducted by Kapti and Yucenur (2006) utilized a potentiometer in the development of an above-knee prosthesis (AKP). The potentiometer was located at the center of the joint, as shown in Figure 2.6, and was utilized to measure the knee joint angle in order to track pre-defined patterns during the gait cycle.

In another study, an agonist-antagonist active knee prosthesis (AAAKP) was designed by Martinez-Villalpando et al. (2008) which used digital encoders to measure ankle angle and motor displacement, and it used hall effect sensors to measure heel strike and spring compression. Also, AAAKP used an inertial measurement unit (IMU) to measure limb acceleration. Different sensory systems were employed by the researchers to provide sufficient input data for controllers, so the prosthetic leg would be able to duplicate the normal gait cycle.

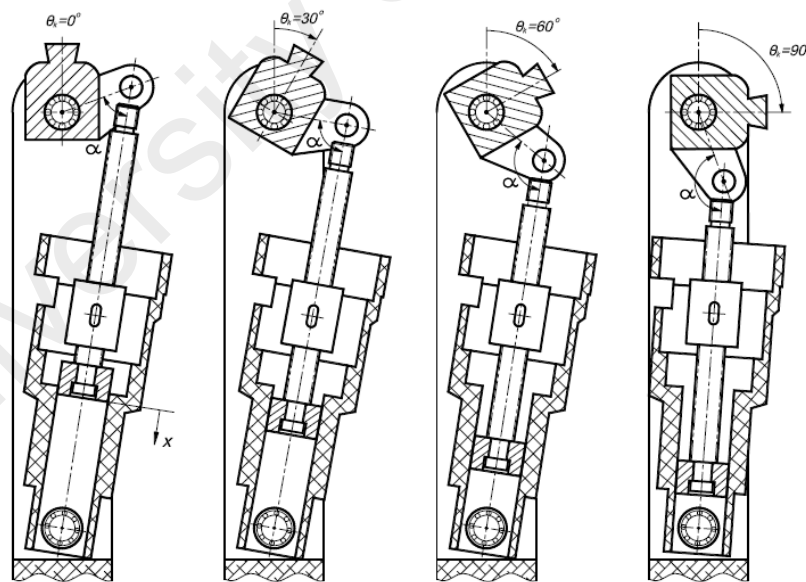


Figure 2.6: The above knee prosthesis (AKP) at different knee flexion angles (Kapti & Yucenur, 2006)

Various types of mechanical sensors such as accelerometers, gyroscopes, and vertical load sensors are used in prosthetic legs to interact with the user and the mechanical leg in order to improve the controllability and stability. Many attempts have been conducted by researchers to enhance the performance of the prosthetic leg. FSR, which is placed under the prosthetic foot, is used to indicate when the heel strike or toe-off during the gait cycle. FSR has several good features such as low cost, relatively thin, ability to generate analog signals and small size (Syrseoudis et al., 2008). Another use of FSR is to measure the pressure distribution patterns corresponding to muscle contraction in the forearm (Li et al., 2012). However, in the transfemoral prosthesis field, FSR is used to detect phases of gait cycle by placing the sensor under the foot, so that it can detect when the foot touches and leaves the ground. Sensors need to be located as close as possible to the residual limb of the amputee to provide sufficient input data to the controller and advance the performance of the prosthesis. In addition, in order to have a real-time detection of the prosthesis activities, sensors need to be in direct interaction with the amputee stump. However, the current techniques have limitations when it comes to direct interaction between the sensory system and the residual limb of the amputee. Thus, some studied attempted to detect the user's intention using electroencephalography (EEG) and electromyography (EMG) to advance the prosthesis's control system.

Beside mechanical sensors, electroencephalography and electromyography are the most recent sensory systems used to improve controlling mechanical legs. In EMG technique, muscle activities are detected using electrodes, as shown in Figure 2.7, and the acquired signal is then fed to the controller. The controller will send a command to the actuator in order to adjust the prosthesis accordingly. EMG signal works as a feedback, which updates

the activities of the user, to the control unit of the prosthesis. Prostheses that are controlled using EMG are called myoelectric control, and they are used, in the field of transfemoral amputation, to do repetitive tasks. Compare to other mechanical-sensor data, EMG control information is considered less robust since EMG signals are noisy.

Amplification circuit is needed in order to eliminate noise from EMG signals which may cause some problems if precautions have not done appropriately. Additionally, electrodes could cause sores for the patient because of movements between the amputee's remaining part of the leg (residual limb) and the socket's wall (Hargrove et al., 2013). Apart from the sores which electrodes cause, sweating, produced due to long contact between residual limb and electrodes, causes discomfort and skin problem. In addition, EMG control method has some notable shortcomings including: 1) massive preparation work is needed to accurately place the electrodes at their proper positions which causes discomfort and skin problems; 2) feature extraction of the EMG signal is computationally expensive; 3) noise could be caused by sweat, mechanical stress and electromagnetic radiation (Li et al., 2012).

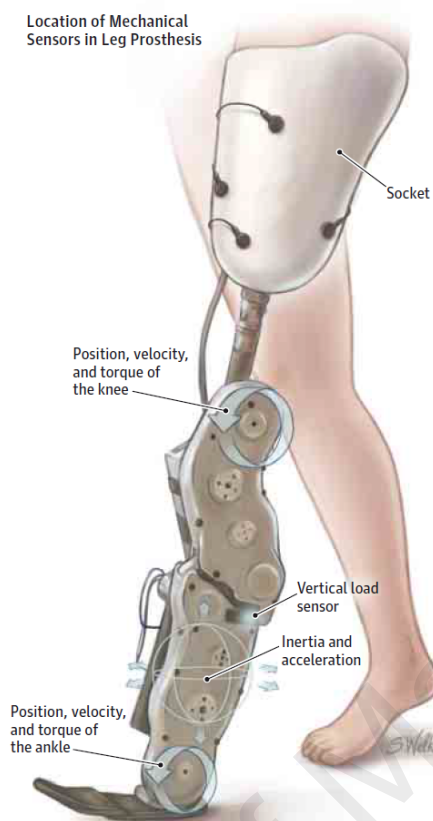


Figure 2.7: Electromyographic (EMG) and Mechanical Sensor (Hargrove et al., 2015)

Electroencephalography (EEG) signal is the electrical activities of the brain recorded by electrodes which are placed on the scalp. The neurons of a human brain process information by changing electrical current flow which generates magnetic and electric fields. EEG technique is used widely in clinical work and the evaluation of brain disorders. Researchers have attempted to use the EEG technique to control prosthetic legs. Due to the short lifespan and the absence of robustness, EEG technique is not a good option to control the prostheses. The amplitude of the EEG signals is very small which makes them contaminated by noise easily (Deepa, Thangaraj, & Chitra, 2010). In addition, the signal-to-noise ratio of the EEG

signals is very small; thus, noise can be generated by the electrodes, cables or the body of the patient (Khatwani, 2013).

Beside EMG and EEG, several works have been proposed to use mechanical sensors to measure force and torque in the prosthesis (Eshraghi et al., 2013). Also, Inertial Measurement Unit (IMU) was suggested to be used to acquire kinetic and kinematic data from the prosthetic leg during amputee movements (Jasni et al., 2016).

Overall, apart from the drawbacks mentioned about EEG and EMG techniques, some health and ethical considerations have to be taken during acquiring data from EEG and EMG electrodes. Moreover, EMG electrodes need to be clean and dry before donning the socket. Thus, it is highly recommended to look for an alternative to replace the current techniques used to interact between the residual limb and control system of the prosthetic leg to ensure better performance that mimics the sound leg.

2.7 Piezoelectric transducers

Many studies have attempted measuring the generated force inside stumps using piezoelectric transducers for both transtibial and transfemoral amputees due to its electro-mechanical feature. In a study conducted by Ali et al. (2013), F-socket transducers 9811E was used to study the interface pressure generated by the transtibial amputees' stumps. The transducers were placed in several positions such as anterior, posterior and lateral to obtain the greatest possible pressure interface between the sockets and stumps. Several trials were conducted to measure the interface pressures during ascending and descending stairs, and the study showed that the interface pressures exist between the socket and stump. Another study attempted to measure the pressure of the transfemoral amputee's stump using

Flexforce network sensors which consist of five Flexforce elements. The result of the study was promising since it could measure the forces applied to the x-direction (El-Sayed, Hamzaid, & Abu Osman, 2014a).

Piezoelectric materials have the capability to act as sensors which encourages researchers to attempt utilizing them in transfemoral prostheses sockets to measure the pressure between the residual limb of the amputee and the wall of the socket. Piezoelectric bimorph can be placed on the wall of the socket, where high interface pressure is expected such as anterior distal and posterior regions, which is directly in contact with the residual limb (Ballas, Schlaak, & Schmid, 2006). A feasibility study was conducted to identify prosthetic knee movements via pattern recognition of mechanical responses of force sensing resistor (FSR) and piezoelectric sensors (in two different setups) attached to the socket's wall of a prosthesis. The first setup consisted of two FSR attached to the posterior and interior of the socket's wall whereas the second setup consisted of three piezo sensors attached to the anterior proximal, anterior distal and posterior of the wall of the fabricated socket. The technique was validated by several movements such as stair ascending and gait cycle as shown in Figure 2.8 and Figure 2.9, respectively.



Figure 2.8: Locations of FSRs attached to the socket's wall(El-Sayed et al., 2015)

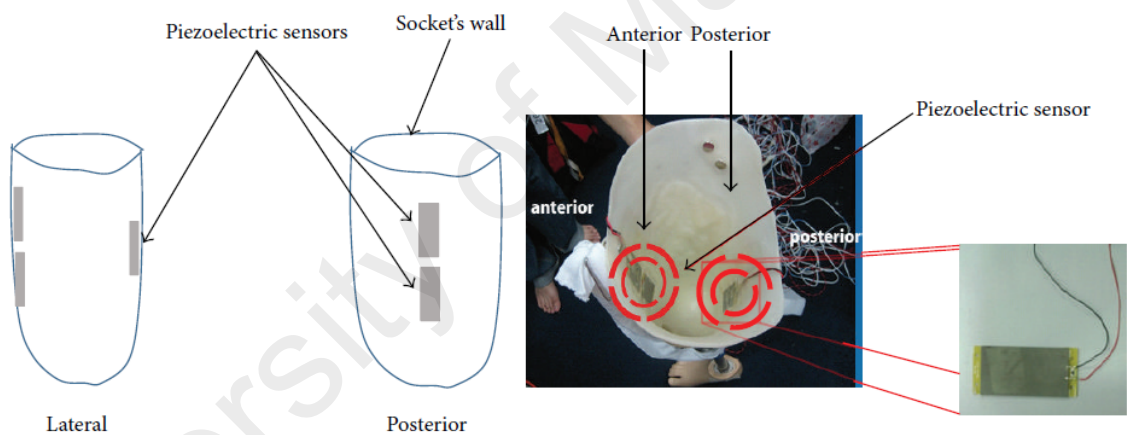


Figure 2.9: Locations of piezo sensors inside the socket at anterior and posterior sites (El-Sayed, 2015)

The study showed that piezoelectric sensors could identify a wide range of measurements including phases of different movements such as mid swing and terminal swing, pre-full standing and stair ascent. On the other hand, FSR has some measurement limitations and could only estimate the pre-full standing phase at sit-to-stand movement and the stance

phase at the gait cycle; thus, FSR would be useful to act as a trigger in the knee movement such as walking, sit-to-stand, and stair ascending (El-Sayed et al., 2015).

An efficacy study was conducted by Jasni et al. (2016) to develop a sensory system that uses piezo transducers inside a prosthetic socket. The piezo transducers are directly in contact with the amputee's residual limb. The study's results suggested that piezo transducers need to adopt Cushion-All with Fit size (CA FIT) cantilever in order to be mounted on the socket's wall. In addition, sensors need to be positioned in a zigzag orientation in order to cover active regions of the Quadriceps and Hamstring muscles, and the proposed design was proven to be effective for a transfemoral prosthesis.

In a study conducted by Maurizio et al. (2017), piezoelectric sensors were utilized to measure normal pressure (both dynamic and static) in order to monitor the stress caused by the contact between prosthesis' wall and the residual limb of the amputee, as shown in Figure 2.10 Another study, conducted by Lorenzelli et al. (2017), developed a tri-axial force piezoelectric sensor which could map the interaction forces between the socket and the leg. The contribution of the study was to enhance and optimize the design of a transfemoral socket.

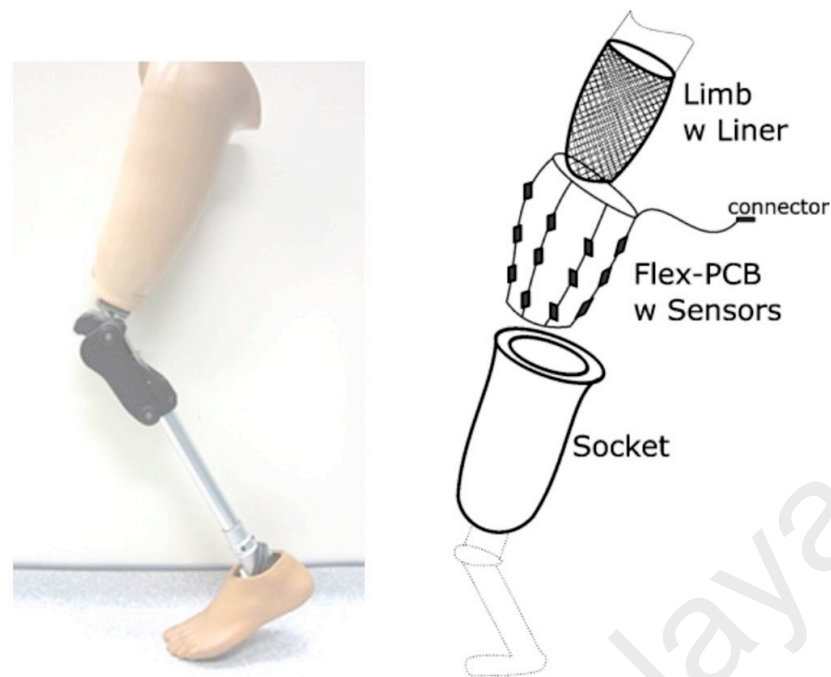


Figure 2.10: Flexible printed circuit board integrated with piezoelectric sensors to measure the stress between the socket's wall and the residual limb of the amputee (Maurizio et al., 2017)

2.8 Pattern recognition in prosthetic limbs

Pattern recognition classifies data into different classes based on their features. Mainly in pattern recognition, the classification methods are divided into two categories: supervised and unsupervised classification. In the field of prosthetic limbs, pattern recognition is considered a promising approach which could detect the user's instantaneous movements from EMG signals and control set of motions (Smith et al., 2011). B. Hudgins (1993) introduced the first real-time pattern recognition approach with high accuracy and performance. This study utilized the use of multilayer perceptron neural network classifier with a set of simple time-domain statistics.

In another study, four different motions were classified with an error rate of 10% using a Gaussian mixture model with EMG for upper limb prostheses (Huang et al., 2005). This

study attracted the attention of researchers and renewed their interest in using a pattern recognition approach to control prostheses. Generally, the pattern recognition approach starts by segmenting data and then extracting useful information from the segmented data. Finally, the pattern recognition algorithm (classifier) will categorize the input data into output categories.

2.8.1 Data windowing

It is commonly believed that the raw data of piezoelectric sensor signals are useless input for pattern recognition approach due to its random nature. Thus, signal segmentation or data windowing is required to extract descriptive features from raw data. These descriptive features will then be fed to a classification algorithm to determine a class of the raw data. There are mainly two approaches of data windowing, namely: 1) overlapping and disjoint segmentation. The former one depends on the segmentation length, processing time and the increment length while the latter relies only on the segmentation length and processing time. Englehart and Hudgins (2003) introduced the overlapping segmentation technique in their work.

Figure 2.11 shows the overlapping technique introduced in their work. The length of the segment is T_a . In order to find the number of samples, the segment length T_a is multiplied by the sampling rate. To find the number of new samples which will be segmented and analysis next, the sampling rate is multiplied by the window increment (T_{inc}). T_{inc} needs to be shorter than T_a in order to produce the best possible stream processing. T_d is the signal processing time, which is the time required by a processor to segment and analyze the previous window.

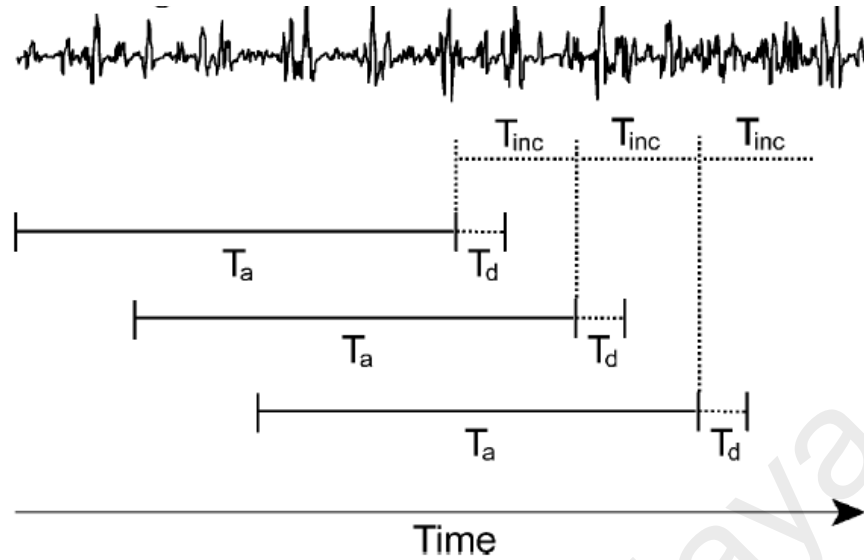


Figure 2.11: The overlapping method for segmenting data (Smith et al., 2011)

The disjoint method divides a sequence of data into disjoint subsets (segments). Figure 2.12 shows the disjoint method for segmenting a sequence of data, where PT is the processing time and S is the segment length.

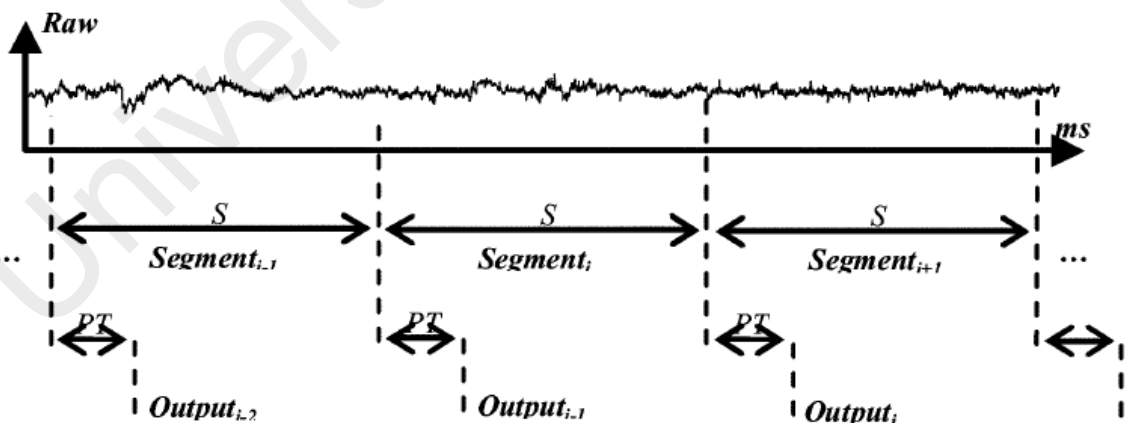


Figure 2.12: The disjoint method for segmenting data (Oskoei & Hu, 2008)

2.8.2 Feature extraction

Pattern recognition consists of three main stages (data windowing, feature extraction, and classification). Figure 2.13 shows feature extraction which is one of the main procedures in pattern recognition. Feature extraction obtains useful information from the subsets of the data sequence. Thus, several studies have been conducted to extract features from the signals in the field of pattern recognition such as time-domain feature and frequency-domain features (Liu et al., 2013). Time and frequency analysis methods are widely used in the field of pattern recognition because of their noticeable physical interpretation and relatively low computational cost. In the time-domain analysis, for instance, slope sign changes (SSC), mean absolute value (MAV), zero crossing (ZC), root mean square (RMS), and mean absolute value slope (MAVSLP) are among the most used time-domain features. In the frequency-domain analysis, cepstral coefficients and Fourier transform coefficients are the common feature extraction methods. Recently, researchers have combined the two methods (time and frequency domain analysis) to introduce a new analysis method called time-frequency method. Wavelet package, short time Fourier transform, and wavelet are the most common features in time-frequency method (X. P. Chen, Zhu, & Zhang, 2010).

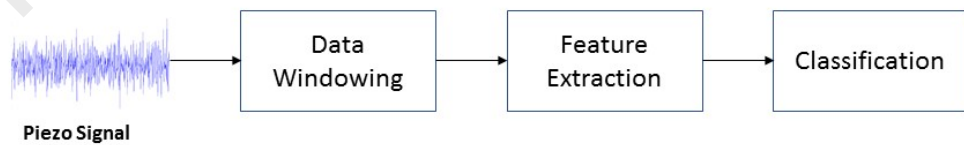


Figure 2.13: Block diagram of piezo signal classification based on pattern recognition

Pattern recognition and feature extraction have been used widely in the field of prosthetic limbs. In a study conducted by Oskoei and Hu (2008), frequency-domain and time-domain features were used to classify hand's movements using myoelectric control. Time-domain features such as variance, root mean square, mean absolute value, and zero crossing were chosen in this study. Furthermore, frequency-domain features were used in their work such as power spectrum, mean of signal frequency and autoregressive coefficients.

In a study conducted by Angkoon, Chusak, and Pornchai (2009), six upper limbs motions were classified by extracting frequency-domain and time-domain features from eight different EMG electrodes. Time-domain features such as mean absolute value, integrated EMG, mean absolute value slope, simple square integral (SSI), zero crossing and root mean square were extracted from the eight electrodes. Besides, frequency-domain were also evaluated. Autoregressive coefficients (AR), and modified median frequency (MMF) were extracted from the EMG electrodes. The classification rate validated by Leave-One-Out showed that MAV, ZC, SCC, AR, and RMS have the cleanest level of signal-to-noise ratio (SNR).

In another study conducted by Xi et al., (2017), a wearable leg EMG sensors were utilized to monitor activities and detect falling using pattern recognition. The study tested several features (time-domain and frequency domain). Time-domain features consisted of variance, zero crossing, integral of absolute value (IAV), number of turns (NT) or slope sign changes, wavelength (WL), and mean of amplitude (MA). Frequency-domain features, on the other hand, consisted of zero crossing of wavelet coefficient (ZCWT), mean frequency (MNF), energy of wavelet packet coefficient (EWP), and energy of wavelet coefficient (EWT). The

results show that frequency-domain features require more time compare to time-domain which make them not suitable for instantaneous monitoring and fall detection.

The following are the most common time-domain and frequency-domain features which were used in this work:

2.8.2.1 Mean Value

Mean value can be calculated by taking the average of the piezoelectric signal of each window. It requires low memory space and low computational power to be obtained which makes it one of the most popular time-domain features. The formula of mean value can be expressed as (Geethanjali & Ray, 2014):

$$Mean = \frac{1}{N} \sum_{n=1}^N x_n \quad (1)$$

where N is the length of the piezoelectric signal segment, and x_n is the n sample of the piezoelectric segmented signal

2.8.2.2 Standard deviation

Standard deviation is used to measure and quantify the amount of variation of a set of data relative to its mean value. Standard deviation is calculated as the square root of the variance. It is defined as follows (Angkoon et al., 2009):

$$SD = \sqrt{\frac{1}{N} \sum_{n=1}^N (x_n - \bar{x})^2} \quad (2)$$

where N is the length of the piezoelectric signal segment whereas x_n and \bar{x} are the n sample of the piezoelectric segmented signal and the mean of the signal, respectively.

2.8.2.3 Skewness

Skewness is a statistical term which used to measure the asymmetry of a data from the normal distribution. There are three types of skewness values which can be positive, undefined and negative. The positive value indicates the data are spread more towards the right side and it is called right skewness. On the other hand, the negative value indicates that the data are spread more towards the left side; therefore, it is called left skewness. When the value of the skewness is zero, it indicates that the data are normally distributed around their mean. The formula of skewness is expressed as (Riillo et al., 2014):

$$Skewness = \frac{\sum_{n=1}^N \frac{(x_n - \bar{x})^3}{N\sigma^3}}{N\sigma^3} \quad (3)$$

where \bar{x} is the mean of the segmented signal, σ is the standar deviation of the segmented signal and N is the number of samples.

2.8.2.4 Variance

Variance is used to measure the spread of data samples (numbers) from their mean. It can be calculated by subtracting each sample of the data from its mean value, squaring the difference, summing all the squared differences and dividing the summation by the number of samples. Variance is defined as (Xi et al., 2017):

$$VAR = \frac{\sum_{n=1}^N (x_n - \bar{x})^2}{N} \quad (4)$$

where N is the length of the piezoelectric signal segment whereas x_n and \bar{x} are the n sample of the piezoelectric segmented signal and the mean of the signal, respectively.

2.8.2.5 Zero crossing

Zero crossing counts how many times the amplitude of a signal crosses the y-axis (zero). It describes the frequency of the signal. It is defined as follows (Angkoon et al., 2009):

$$ZC = \frac{1}{2} \sum_{n=1}^{N-1} |sgn(x_n) - sgn(x_{n-1})| \quad (5)$$

where sgn is a sign function which is defined as follows:

$$sgn(x) = \begin{cases} 1, & sgn(x) \geq 0 \\ -1, & sgn(x) < 0 \end{cases} \quad (6)$$

2.8.2.6 Root mean square

Root mean square refers to the square root of the mean square of a signal, and it is also called the quadratic mean. The root mean square is referred as standard deviation when the signal has a zero mean. Root mean square can be defined as follows (Hargrove et al., 2013):

$$RMS = \sqrt{\frac{1}{N} \sum_{n=1}^N x_n^2} \quad (7)$$

where N is the length of the piezoelectric signal segment, and x_n is the n sample of the piezoelectric segmented signal.

2.8.2.7 Number of peaks

One way to distinguish a signal is to derive its number of local maxima peaks. Local peaks are those with value higher (depending on the threshold) than their neighboring samples. MATLAB function called `findpeaks` was used twice to find the number of local peaks. In the first time, it found the local maxima peak for the positive amplitude. Then, the signal was inverted by multiplying it by -1 and the function was called for the second time to count the

number of local peaks for the negative part of the signal. The amplitude threshold (minimum peak height) was set to 0.1 V and the distance threshold (minimum distance between two peaks) was set to 100 ms.

2.8.2.8 Kurtosis

Kurtosis is used to measure the distribution of data based on extreme values of the tail. When the value of kurtosis is positive it indicates that the tail of the data is exceeding the tail of the normal distribution (pointy tail). On the other hand, when the value of kurtosis is negative it indicates that the tail of the normal distribution is pointier which means the tail of the measured data is less extreme. Kurtosis's formula is shown below (Dawley et al., 2013):

$$kurtosis = N \sum_{n=1}^N \frac{(x_n - \bar{x})^4}{\sigma^4} \quad (8)$$

where \bar{x} and σ the mean and standard deviation of the segmented signal, x_n is the n sample of the segmented signal and N is the number of samples.

2.8.2.9 Integral of absolute value

In discrete signals, integral of absolute value is calculated as the summation of each sample absolute value of the signal and divided by the total number of samples (N). The formula of IAV is expressed as (Xi et al., 2017) :

$$IAV = \frac{1}{N} \sum_{n=1}^N |x_n| \quad (9)$$

where x_n is the n sample of the segmented signal and N is the number of samples.

2.8.2.10 Simple square integral

The energy of a signal is used as a feature using the simple square integral. The simple square integral is the summation of the square of the sample's absolute value. SSI is a popular feature used in pattern recognition to detect muscle expansion and contraction. The equation of SSI is defined as (Xi et al., 2017):

$$SSI = \sum_{n=1}^N |x_n|^2 \quad (10)$$

2.8.2.11 Mean absolute value

The mean absolute value is calculated by taking the average of the absolute value of each sample. It is similar to the average rectified value which averages the rectified signal (absolute values). Mean absolute value is used widely in machine learning and pattern recognition due to its computational simplicity. MAV is expressed as (Smith et al., 2011):

$$MAV = \frac{1}{N} \sum_{n=1}^N |x_n| \quad (11)$$

2.8.2.12 Slope sign change

Another method to describe the frequency of the signal is by counting the slope sign changes. Slope sign change is also called the number of turns (NT). Slope sign change formula is defined as follows (Angkoon et al., 2009):

$$SCC = \sum_{n=2}^{N-1} [f((x_n - x_{n-1}) \times (x_n - x_{n+1}))]$$

$$f(x) = \begin{cases} 1, & \text{if } x \text{ slope changes} \\ 0, & \text{if no changes in slope occurs} \end{cases} \quad (12)$$

where x_n is the n sample of the segmented signal and N is the number of samples.

2.8.2.13 Mean Frequency

Mean frequency (MNF) is considered as a frequency-domain feature which is deployed from the power spectrum of the piezoelectric sensor. It is defined as the sum of the piezoelectric signal power spectrum multiplied by the frequency and divided by the summation of the signal spectrum intensity. The formula of the MNF is defined as follows (Thongpanja, Phinyomark, Phukpattaranont, & Limsakul, 2013):

$$MNF = \frac{\sum_{j=1}^M P_j f_j}{\sum_{j=1}^M P_j} \quad (13)$$

where f_j is the frequency value, p_j is the power spectrum of the signal and M is the length of the frequency bin.

2.8.2.14 Median Frequency

Median Frequency (MDF) is also considered as a frequency-domain feature which is used to extract information from a signal. Similar to the mean frequency, the median frequency is deployed from the power spectrum of a piezoelectric signal. It can be defined as the value of the frequency which divides the power spectrum of the piezoelectric signal into two equal integrated power regions. MDF is expressed as follows:

$$\sum_{j=1}^{MDF} P_j = \sum_{j=MDF}^M P_j = \frac{1}{2} \sum_{j=1}^M P_j \quad (14)$$

where MDF is the middle value of frequency which divides the signal power spectrum into two equal regions, P_j is the power spectrum of the signal whereas the length of the frequency bin is M (Liu et al., 2013; Thongpanja et al., 2013).

2.8.2.15 Spectral power magnitude

Spectral power magnitude (SPM) is calculated by performing the fast Fourier transform (FFT) for a data segment followed by finding the average of the power spectrum of the FFT segment. In previous studies, SPM has proved that it is an effective frequency- domain feature (Chen & Wang, 2013).

2.8.3 Classification algorithms

Pattern recognition technique is considered as a classification process, which its main aim is extracting patterns from given inputs (features) (Lihong Zheng & Xiangjian He, 2007). The classification algorithm plays a vital role in the overall recognition performance, recognition efficiency and computational complexity (Chen & Wang, 2013). Pattern recognition algorithms are categorized into two categories based on the learning method. The first category is unsupervised learning which is used to solve problems such as clustering and association. The second category is supervised learning which its algorithms used to solve problems such as classification and regression.

In the recent years, the pattern recognition approach has been used widely in the field of prosthetic limbs using EMG and EEG signals. However, most of the applications are based on upper limb application. In a study (Chen & Wang, 2013), a wireless surface EMG system was developed to classify Chinese number gestures. In this study, several pattern recognition algorithms were tested and compared. Linear discriminant analysis (LDA), k-nearest neighbor (k-NN), support vector machine (SVM) with different kernels, and quadratic discriminate analysis (QDA) were utilized to classify number gestures from zero to nine. The results showed that SVM and QDA could achieve classification accuracies above 95% while k-NN and LDA were less robust compared to SVM and QDA.

In another study conducted by Riillo et al. (2014), an EMG-based recognition system was employed to classify hand gestures of transradial amputees and healthy subjects. Three pattern recognition algorithms (SVM, LDA and artificial neural network (ANN) were compared to accurately recognize five hand gestures. Artificial neural network algorithm achieved the highest average classification accuracy (88.81% with a standard deviation of 6.58) with healthy subjects using root mean square (RMS) and Willison amplitude (WA) features. The same algorithm (ANN) and features (RMS and WA) achieved 92.04% classification accuracy with transradial amputees.

Table 2.1 presents a summary of the reviewed literature. It can be seen that all of the literature used EMG signals to classify activities of upper and lower limbs using the pattern recognition technique. Time-domain features were preferable due to their short processing time compared to frequency-domain features, computing simplicity, and low memory space.

Table 2.1: Summary of the state-of-the-art literature review on the pattern recognition technique with prosthetic applications

Study	Type of application	Control method	Time-domain features	Frequency-domain features	Window Length (ms)	Classification algorithm	Classification accuracy and other remarks
(Oscoei & Hu, 2008)	Prosthetic hand	Myoelectric	ZC, RMS, VAR, MAV, WL, and SSC	PS, AR2, AR6, median and mean of the signal frequency	50-500	SVM, LDA and multilayer perceptron (MLP)	SVM offered robust performance with exceptional accuracy
(Angkoon et al., 2009)	Arm gestures	EMG	RMS, VAR MAVS, SSC, ZC, WL, and histogram	AR, modified mean frequency, and modified median frequency	256	Noise removal algorithm	MAV, ZC, SCC, AR, and RMS have the cleanest level of signal-to-noise ratio
(Khokhar, Xiao, & Menon, 2010)	Wrist exoskeleton	EMG	RMS	AR model coefficients	250	SVM	Accuracy for 19 classes is 88% and for 13 classes 96%
(Chen & Wang, 2013)	Hand gestures	wireless surface EMG	MAV, ZC, SSC and MAV ratio	Spectral power magnitudes	64	k-NN, LDA, QDA, and SVM	SVM and QDA classified with accuracies above 95%
(Riillo et al., 2014)	Hand gesture	EMG	Mean, RMS, WA, SSC, SSI, PCA, and VAR	NA	300	SVM, ANN, and LDA	ANN with RMS and WA achieved the highest accuracy

Table 2.1 continued

Study	Type of application	Control method	Time-domain features	Frequency-domain features	Window Length (ms)	Classification algorithm	Classification accuracy and other remarks
(Geethanjali & Ray, 2014)	Prosthetic hand	EMG	MAV, ZC, SSC, WL, MAVS, VAR and RMS	NA	256	Simple logistic regression, decision tree, NN, LDA, and logistic model tree	Five ensembles groups were obtained from the time-domain features and NN and LDA offer the highest classification accuracy.
(Xi et al., 2017)	Wearable leg sensors	EMG	VAR, ZC, SSC, Mean of Amplitude and Histogram	MF, AR coefficients, Energy of Wavelet Coefficient	NA	Gaussian kernel SVM and Fuzzy Min-Max NN	Gaussian kernel SVM with frequency-domain achieved with the highest accuracy (97.35%) but with high calculation time

* Electromyography (EMG); zero crossing (ZC); root mean square (RMS); variance (VAR); mean absolute value (MAV); waveform length (WL); mean frequency (MF); slope sign change (SSC); autoregressive (AR); neural network (NN); linear discriminate analysis (LDA); quadratic discriminate analysis (QDA); support vector machine (SVM); k nearest neighbor (k-NN); power spectrum (PS); principle component analysis (PCA); simple square integral (SSI); artificial neural network (ANN)

2.9 Summary

In this chapter, a literature review of the existing technology of transfemoral was discussed and analyzed. This chapter illustrated a brief review of the existing technology of transfemoral prosthesis. Section two and three discussed the biomechanics of sitting and standing. Sensory systems used in transfemoral prostheses were described in the fourth section of this chapter. Besides, a literature review of the piezoelectric transducers used in transfemoral prostheses was discussed. The stages of the pattern recognition process were described in this chapter as well as the most popular features and classification algorithm used in pattern recognition.

A transfemoral prosthesis is required to assist amputees to perform the activity of daily living (ADL). Although the passive prosthesis has advantages such as low cost, robustness, light weight and durability, it has some drawbacks which can be summarized as follows:

1. Single axis prosthesis has no stance control and is free-swinging which means amputees need to use their muscle to control and stabilize the prosthetic leg.
2. The hydraulic passive prosthetic leg requires frequent maintenance and weights more compared to other passive legs
3. The manual locking passive prosthesis requires high energy to perform activities which leads to fatigue
4. The weight-activated stance-control prosthesis requires frequent and accurate adjustments to ensure the lock is working properly. Also, it has only one walking speed.

5. The current passive prostheses do not adequately fulfil the needs of amputees during sitting down and standing up owing to the lack of external power which assists the elevation of the body weight and the high consumption of metabolic energy.

On the other hand, the active prosthesis consumes less metabolic energy and offers better performance owing to the embedded microprocessor, sensors, and actuators which allow to adjust the impedance. However, the recent active prosthesis cannot support the amputee to perform energy-demand activities such as stair climbing and sit-to-stand. Powered or motorized active prostheses were introduced to overcome these shortcomings. The powered active prostheses are controlled using embedded sensory systems located away from muscles which measure different parameters such as position, force, velocity, phase transitions, and torque to control a prosthesis system. These sensory systems lack the direct interaction with the amputee's residual limb which, as a result, prevents exploitation of the useful information about neuromuscular activities which can be used to derive the user's state of movement instantaneously. Another clinical method to control the motorized prosthesis is to use EEG, however; due to its short lifespan, the absence of robustness, and the high of noise-to-signal ratio, this method is not a good option. Another method to control the powered prostheses is to use surface electromyography (EMG) as its sensory system. However, the EMG approach has some drawbacks which can be summarized as follows:

1. Massive preparation work is needed before donning the socket such as shaving and applying gel.
2. Relative thick electrodes cause pain and discomfort because of movements between the amputee's remaining part of the leg (residual limb) and the socket's wall.

3. Feature extraction of the EMG signal is computationally expensive.
4. Noise could be caused by electromagnetic radiation.
5. Weak signals with microvolt-level.

In order to overcome the drawbacks of the EMG-based control and other mentioned approaches, an alternative has to be suggested. A piezoelectric sensor showed promising results when it comes to the user's state of movement instantaneously via muscle contraction. However, to date, only a few studies have been conducted to investigate the feasibility of piezoelectric sensors to be used in the field of transfemoral prostheses. Some advantages of the piezoelectric sensor are the followings:

- 1- Relatively thin compared to the EMG electrodes which, as a result, causes less sore for the amputee
- 2- Requires less complex amplification circuitry compared to the EMG
- 3- Has voltage range in millivolt
- 4- Require a smaller number of sensors compared to EMG electrode to cover muscle region, thus, requires less feature to be fed the algorithm.

The piezoelectric sensory system is still in its first stage and more work is required to validate and develop the system. Therefore, the use of the pattern recognition technique to classify variations of sitting and standing activities using piezoelectric sensors was proposed in this thesis to investigate if the piezoelectric sensor is a good alternative to control the powered prostheses.

CHAPTER 3: METHODOLOGY

3.1 Introduction

This chapter presents the methods used to conduct the experiment. It first details the materials and sensors configuration and placement utilized in the experiment. Also, it explains data collection methods, experiment setup, and experimental protocol. Furthermore, the data segmentation method, feature selection, and pattern recognition algorithms are explained in details in this chapter.

3.2 Materials

The sensory system of the prosthetic leg consisted of fifteen piezoelectric film sensors (FDT series), manufactured by Measurement Specialties, which have high flexibility. The dimension of the sensors (30mm×15mm×0.028mm) makes them suitable to be placed on the internal wall of a socket and caused no skin impingement pain compared to EMG electrodes. In addition, piezo film sensors generate higher voltage compare to other piezo sensors given the same amount of input force. Figure 3.1 shows one film piezoelectric sensor which was used with the other fourteen sensors.



Figure 3.1: Piezo Film sensor (FDT series, Measurement Specialties Product Guide)

A custom-made socket was fabricated by a certified prosthetist, its type was polypropylene quadrilateral (Jasni et al., 2016). In addition, a hydraulic knee joint (3R60 EBS Pro) manufactured by Ottobock was attached to a solid ankle cushion heel foot. Figure 3.2 shows the fabricated socket attached to the hydraulic knee joint and foot solid ankle cushion heel foot.

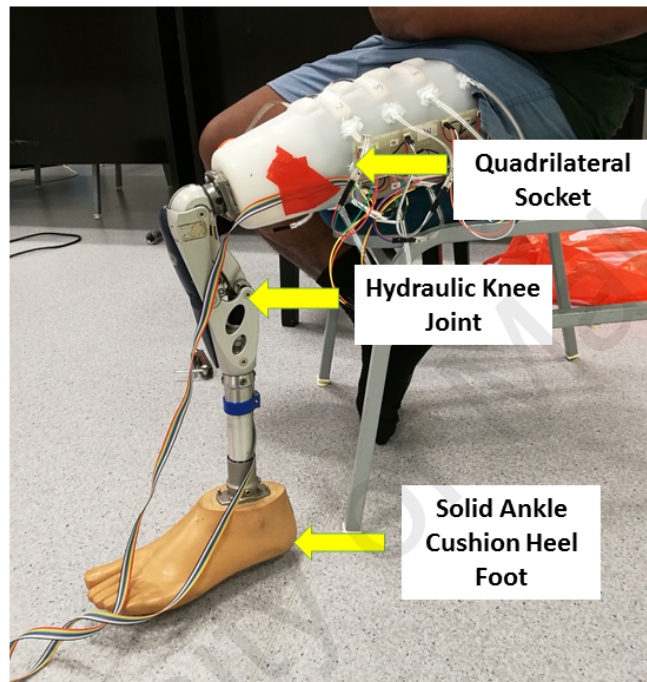


Figure 3.2: The fabricated socket equipped with the in-socket piezoelectric sensors attached to the hydraulic knee joint and the foot solid ankle cushion heel foot

3.3 Sensors configuration and placement

The sensors configuration and placement were adopted from a prior study conducted in our same lab (Jasni et al., 2016). For piezoelectric sensors, the optimal mounting configuration which produced the highest strain for a particular force input was cantilever beam configuration. To enhance the performance of the piezoelectric sensors' output signal, an elastic foundation was added with the cantilever beam configuration. The main

function of piezoelectric sensors is to detect forces applied by the residual limb. Therefore, the location of the sensors was identified to be on active areas and regions that have a high level of muscle contractions. The knee extensor agonist and antagonist muscle groups (quadriceps and hamstring) placement were targeted based on their biggest contraction bulge size and closeness to the skin which eases the measurement process. The areas of quadriceps and hamstring were identified using F-socket sensors (Jasni et al., 2016). Fifteen piezo sensors were placed in zigzag orientation to cover muscle's active regions (quadriceps and hamstring). Seven were placed on the hamstring area (posterior socket's wall) and the remaining eight were placed on the quadriceps area (anterior socket's wall) as shown in Figure.3.3.

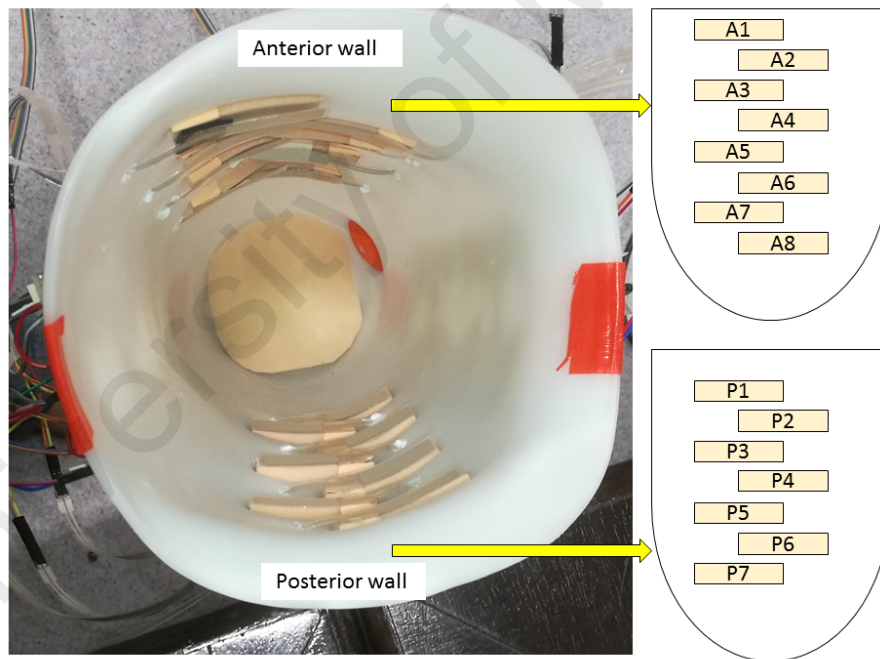


Figure 3.3: The fifteen piezoelectric sensors placed in zigzag orientation on the socket's wall with the added elastic foundation

3.4 Signal conditioning circuitry

Signals acquired from the fifteen piezo sensors went through signal conditioning circuitry. The signals, firstly, were low-pass filtered at a passing frequency of 800 Hz as recommended by the manufacturer to ensure sensors detect small forces (muscle pressure in this case). Secondly, the filtered signals, coming from piezoelectric sensors, were amplified using operational amplifier LM358p (Texas Instruments) by a gain of 11. The filtering and amplification of the signals were conducted via an active pass filter as shown in Figure 3.4.

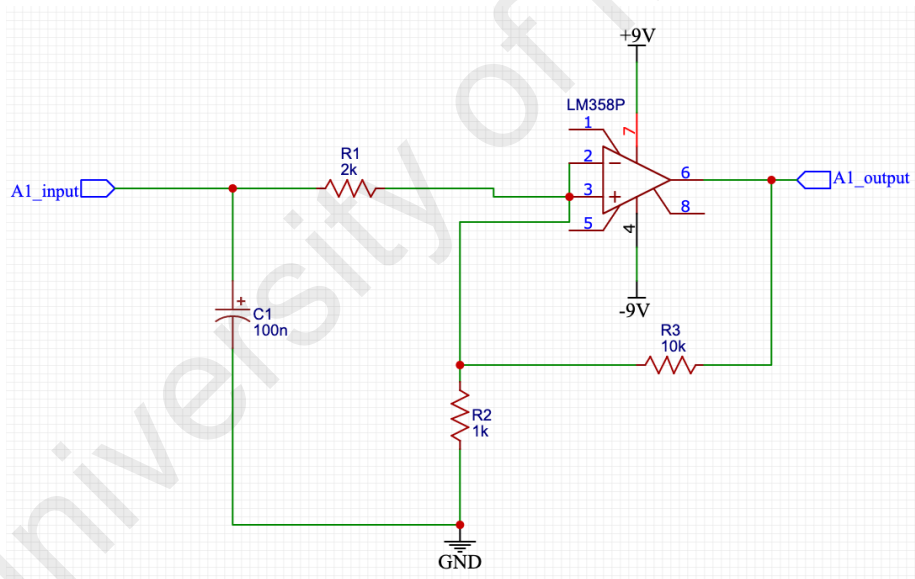


Figure 3.4: An active low-pass filter circuit schematic for the first anterior sensor (A1)

The circuit schematic was then converted into a layout of a printed circuit (PCB) which is shown in Figure 3.5.

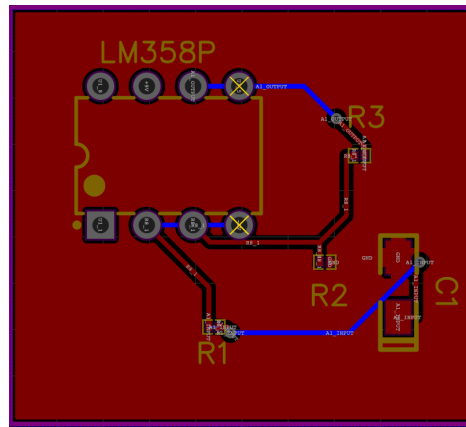


Figure 3.5: The PCB layout of the first anterior sensor (A1)

The cut-off frequency can be calculated using the following equation:

$$F_c = \frac{1}{2\pi R_1 C_1} = \frac{1}{2\pi * 2000 * 100 * 10^{-9}} \approx 800 \text{ Hz}$$

The gain was calculated using the following equation:

$$A = 1 + \frac{R_3}{R_2} = 1 + \frac{10000}{1000} = 11$$

Fifteen active low-pass filters were fabricated separately to simplify troubleshooting, and they were divided into two groups (anterior and posterior). Eight active low pass filters (for anterior sensors) were connected together to reduce wiring mess which may cause accidents for the subject. The remaining low pass filters were utilized for the posterior sensors. The two signal conditioning circuits are shown in Figure 3.6 and Figure 3.7. Two DC power supplies were used to generate +9V and -9V.

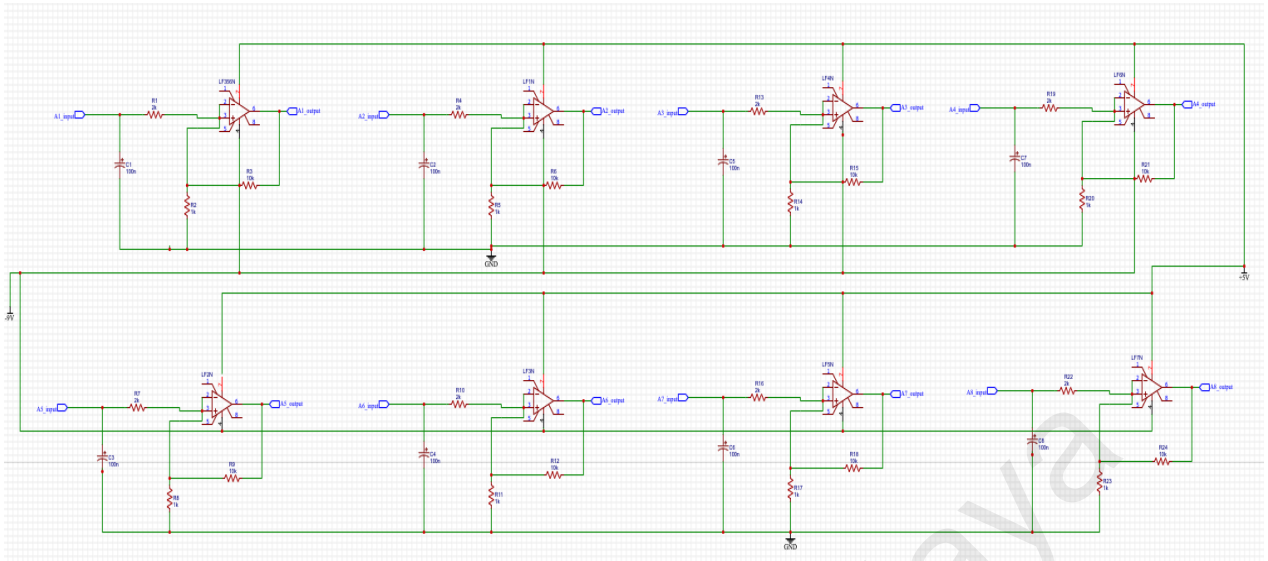


Figure 3.6: The signal condition circuit designed for the eight anterior sensors consisting of eight active low-pass filters

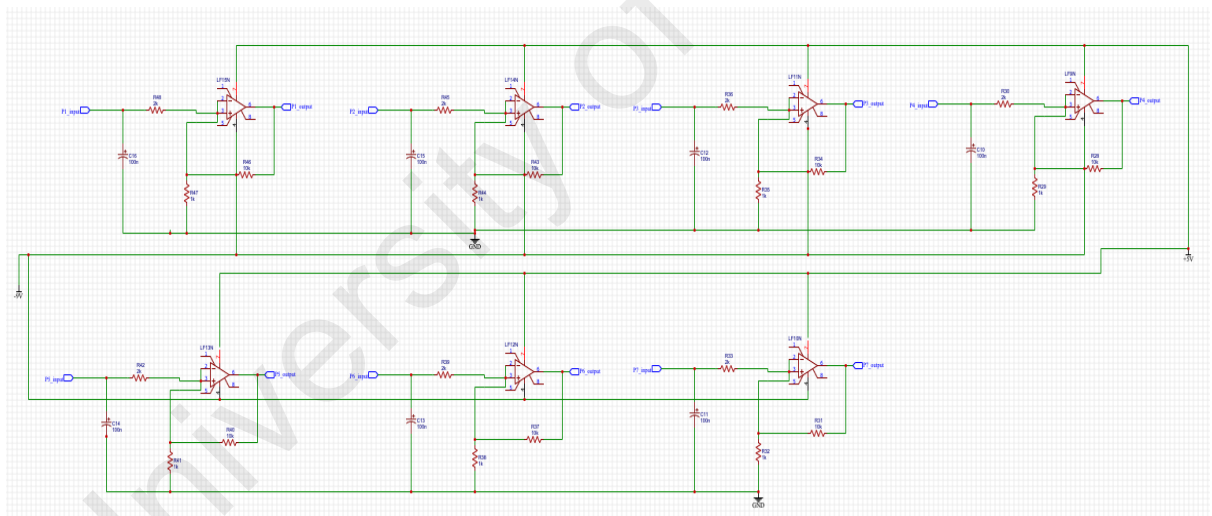


Figure 3.7: The signal condition circuit designed for the seven posterior sensors consisting of seven active low-pass filters

Three different types of cables (twisted pair, coaxial, and ribbon) were tested in order to connect the sensors to the signal conditioning circuits. Ribbon cable was chosen since it has low signal-to-noise ratio and has the least weight and, therefore, exerts the least

tension on the subject. Two ribbon cables were used, the length of each one was three meters.

3.5 Data collection

Two synchronized data acquisition devices (NI 9221, National Instrument) were used to collect the filtered and amplified signals using 12-bit analog-digital converters, and sampling frequencies were set at 1 kHz in both devices. Each data acquisition device had 8 single-ended channels and a signal range up to ± 60 V. A PC was utilized to fetch and store the data using LabVIEW software. The virtual instrument (VI) or the block diagram of the first data acquisition cards, the posterior and anterior sensors, and a trigger is shown in Figure 3.8.

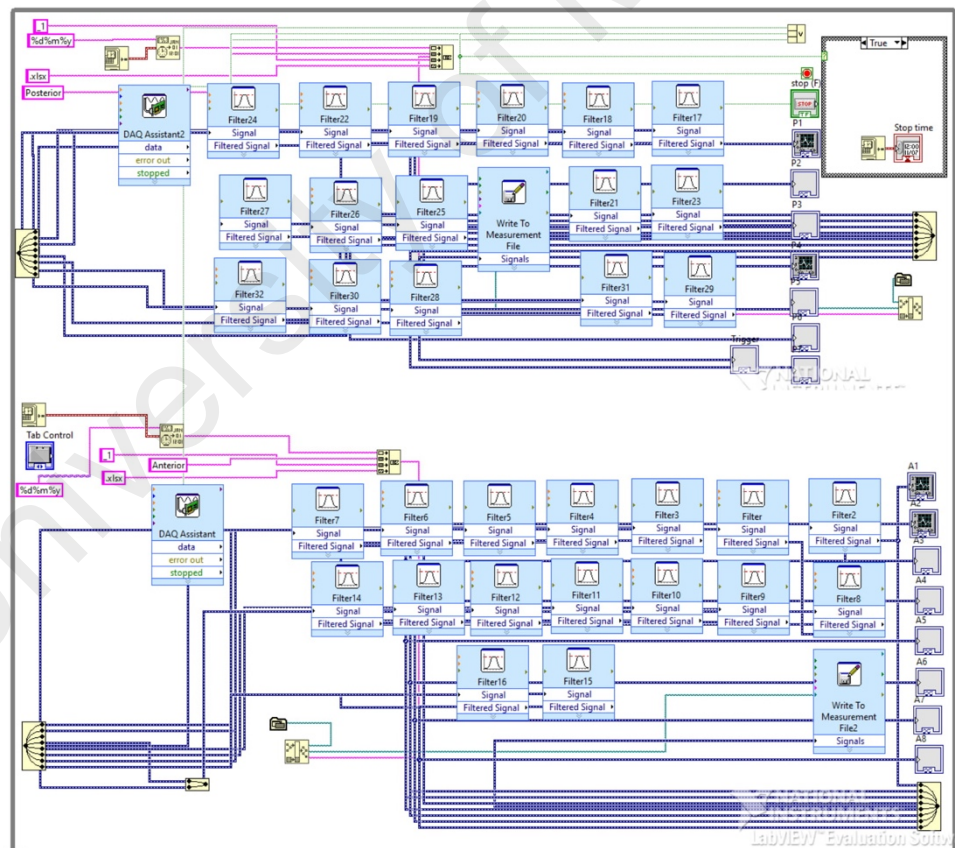


Figure 3.8: LabVIEW virtual instrument of the two data acquisition cards, 15 sensors, one trigger and pass-band filtered

The collected data were pass-band filtered (0.5-20 Hz) using 6th order Butterworth filter (IIR) by LabVIEW software to eliminate noise and get smoother signals. Since muscle activation and deactivation takes place at frequencies up to 20 Hz (Prendergast, Helm, & Duda, 2005), the cut-off frequency was set to 20 Hz. The data acquisition devices, signal conditioning circuits, and the prosthesis are shown in Figure 3.9.

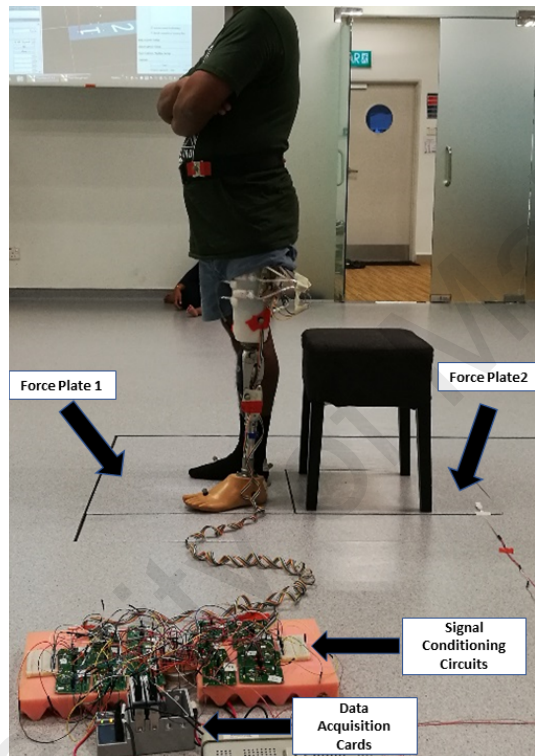


Figure 3.9: A transfemoral amputee donning the in-socket based piezoelectric sensory system and the data acquisition cards connected to the signal conditioning circuits

The experiment was conducted in motion analysis lab of University of Malaya which was equipped with two force plates. Ground reaction forces of the subject were measured using these two force plates at 1 kHz sampling rate of using VICON Nexus (1.8.5) software. The first force plate was placed under the subject feet while the second one was placed under the armless chair. The second force plate was placed under the chair to

detect the seat-off and seat-on transitions which were used to determine phases of sitting and standing (Kralj et al., 1990). Figure 3.10 shows the graphical user interface of VICON Nexus and the two force plates.

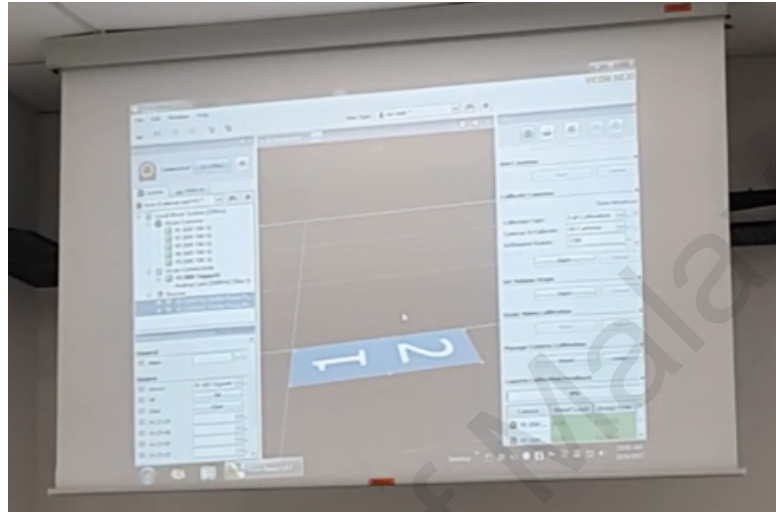


Figure 3.10: The Graphical User Interface (GUI) of VICON Nexus software (Version 1.8.5) used to collect data from the two force plates

The data of the two systems (LabVIEW and VICON Nexus) were synchronized using a trigger switch (piezoelectric sensor) placed on the first force plate and connected to one of the data acquisition cards (DAQ). Before each activity, this sensor was knocked which caused the GRFs of the first force plate to pulse (signal marker) due to the force applied at the same time it made a pulse in LabVIEW system since the sensor was connected to the DAQ. Figure 3.11 shows the trigger switch (sensor) placed on force plate 1 and connected to the data acquisition cards.

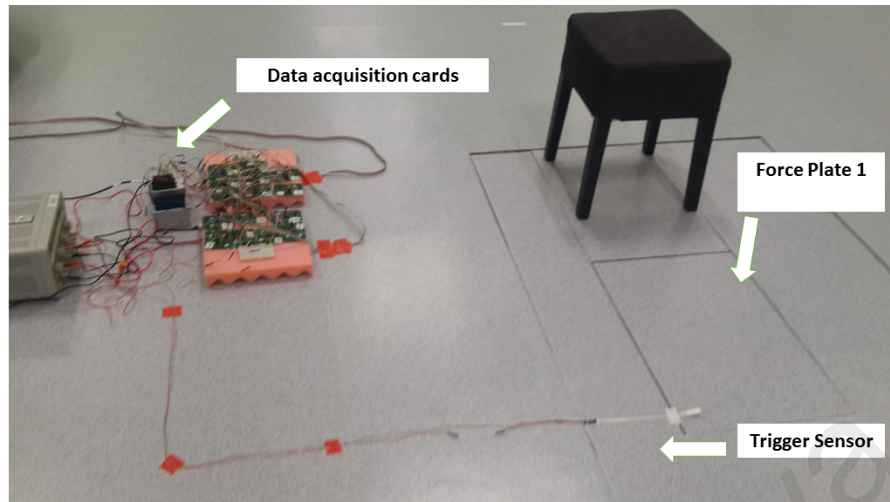


Figure 3.11: Trigger sensor to synchronize LabVIEW and VICON Nexus

3.6 Experiment setup

A 36-year-old male unilateral transfemoral amputee (left leg), of height 174.5cm and weight 789.44 N was recruited. The subject was healthy (in a good mental condition) and had no physiological or other physical problem otherwise. He was a user of a transfemoral prosthetic leg for 17 years. A new user of a transfemoral prosthesis was excluded from this experiment to avoid accidents during the experiment and to ensure that sensors' signals come from the activities only, since stabilizing and balancing during performing the activities could cause uncertainty (noise) for the algorithm. The subject signed a written informed consent approved by the Medical Research Ethics Committee of the University of Malaya Medical Center to participate in this experiment.

3.6.1 Experimental protocol

The subject was given time (around one hour before each session) before conducting the experiment to walk, sit and stand while donning the prosthetic leg in order to get familiar with the prosthesis and ensure the performed activities were similar to his daily

activities. The subject was instructed to perform six activities using an armless chair (42 cm height, in the recommended range of Demura and Yamada (2007) while donning the socket. An armless chair was chosen to make the subject depend only on his leg's muscles.

Prior to performing each activity, as a signal cue for synchronization of data collection, a handphone was set to ring three times. When the phone rang for the first time, the two systems (LabVIEW and VICON) started collecting data. The second time the phone rang was after 5 seconds (to allow the two systems settled from overshooting due to turning the systems on), after hearing the second alarm one person was assigned to hit the trigger switch. The purpose of hitting the trigger sensor was to synchronize the two systems. The third time the phone rang was 5 seconds after hearing the second alarm sound. After hearing the third alarm sound, the subject had to perform the assigned activity. After performing the assigned activity, data collection from the two systems were stopped.

The subject was requested to perform the activities shown in Figure 3.12: 1) Sit-to-Stand, here the subject was instructed to stand up from a stationary position, 2) Stand-to-Sit, here the subject was requested to sit down on a stationary chair from an upright position, 3) Dynamic Sitting, here the subject was expected to have minimum to average lower body movements while sitting down on a chair, 4) Dynamic Standing; where the subject was allowed to shift his weight between the legs with minimal movement while standing upright, 5) Static Sitting; where the subject sat in a rigid position with no bodily movements, and 6) Static Standing ; where the subject stood still in an upright position in the same spot with no bodily movements.

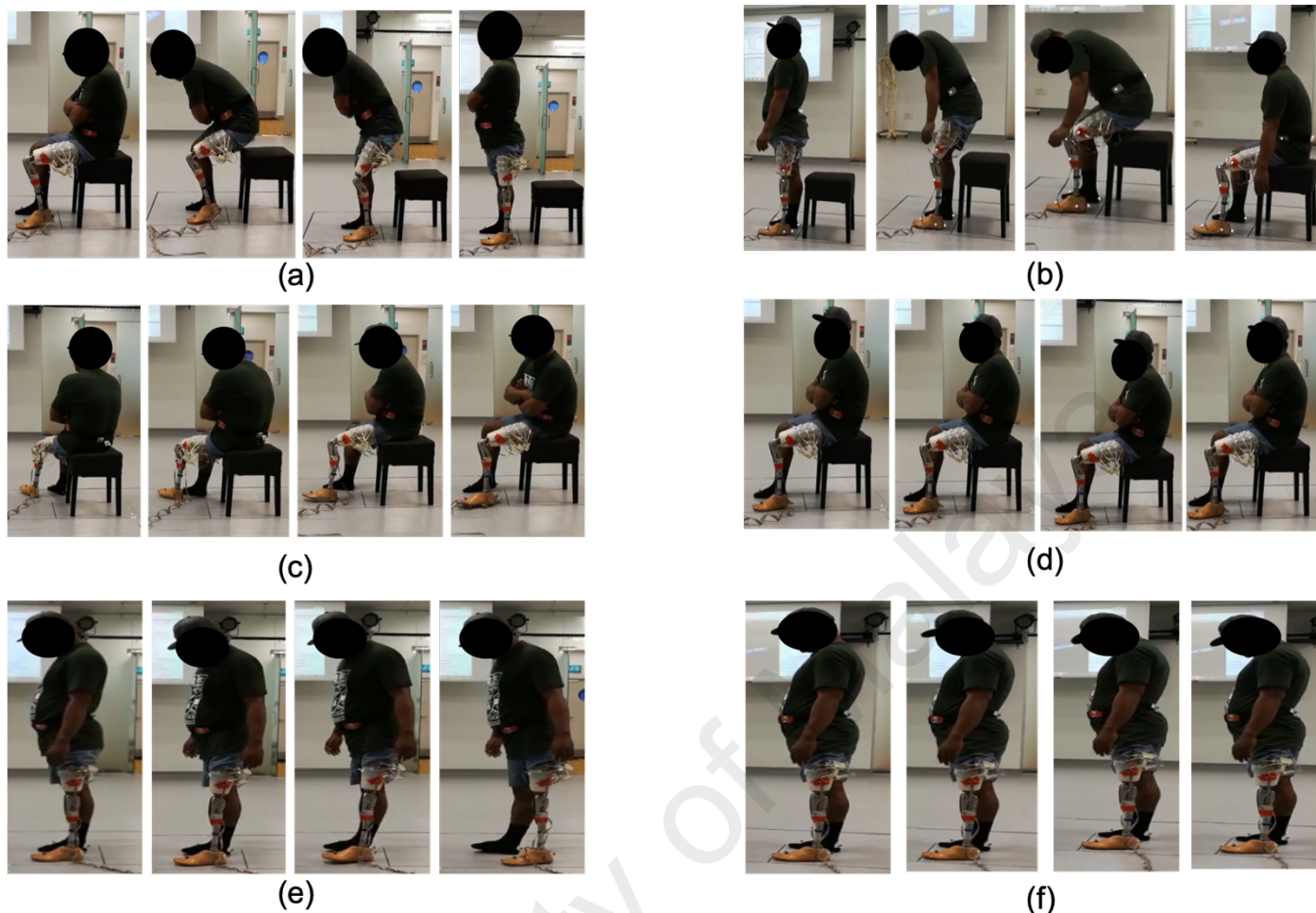


Figure 3.12: Illustration of the activities performed by the subject: (a) Sit-to-stand, (b) stand-to-sit, (c) dynamic sitting, (d) static sitting, (e) dynamic standing and (f) static standing

The six activities were tested in this study, and a total of 360 activities, as summarized in Table 3.1, were performed in three days, each day consisted of two sessions. In each session, 60 activities were performed (ten of each type) and a 30-minute break was given between sessions to avoid fatigue. The number of repetitions for each activity was set to 60 since the learning curve saturated at 46 repetitions. After 46 repetitions, the classification accuracy did not improve which indicated that the training samples are enough, therefore; 80% of the data was utilized for a training set (48 repetitions for each activity) and 20% was held out for a testing set (12 repetitions).

Table 3.1: Experiment protocol of activities

No.	Activity	Number of Repetition
1	Sit-to-Stand	60
2	Stand-to-Sit	60
3	Dynamic Sitting	60
4	Dynamic Standing	60
5	Static Sitting	60
6	Static Standing	60
Total		360

3.7 Data windowing and feature selection

The pattern recognition technique's first stage is to preprocess the data which starts by filtering the sensors' signals from noise and followed by amplifying the signals. After that, the signals are fetched and stored in a PC using data acquisition cards. Then the data is segmented using windowing techniques. At this stage, the features are ready to be extracted from each data window. All the features were normalized in order to have the same scale and eliminate biases. After feature extraction comes the model selection, in this stage a classification algorithm needs to be selected, and after that the model is ready to train. After the training comes the model evaluation which tests the model performance using validation methods. If the model performance is not satisfactory, the parameters of the model will be retuned and go back to the training. However, if the model gives a good

classification accuracy, the model can be used for prediction (generalization). The flow chart of the pattern recognition technique is shown in Figure 3.13.

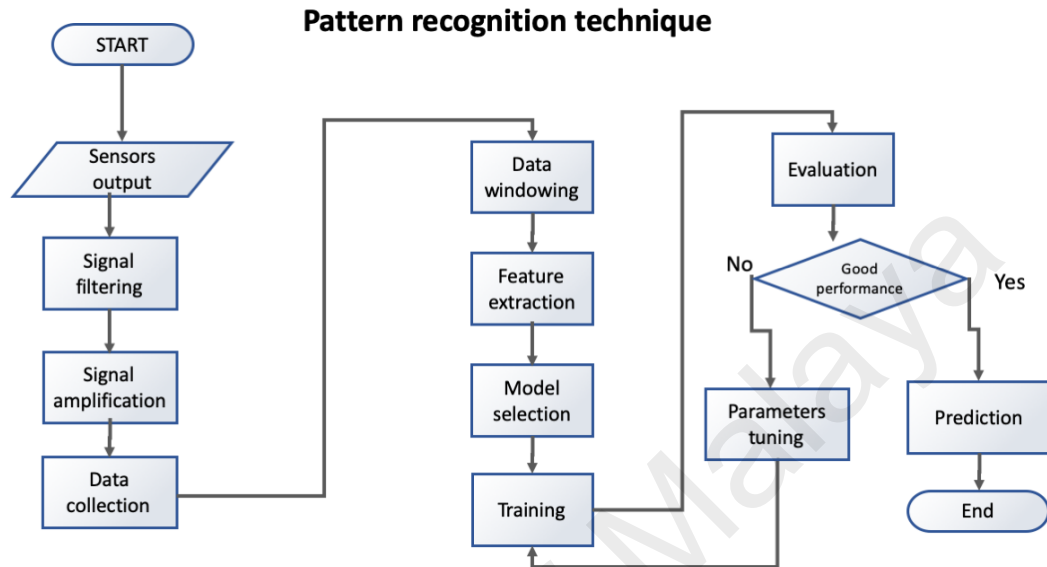


Figure 3.13: The flowchart of the pattern recognition technique

The overlapping technique was used to segment the data using different window lengths (150, 200, 250, 300, 350, 400, 450, 500, 550 and 600 ms), and in order to fulfill real-time requirements of controlling a prosthesis, a delay of 100 ms between two overlapped windows was chosen (Riillo et al., 2014). Different segmentation lengths were used for investigating the effects of window size on the classification accuracy.

Features have to present the properties and characteristics of a signal for different sitting and standing activities and computational load needs to be considered (Oskoei & Hu, 2008). In this work, features were obtained from each time window and were concatenated together to form a feature vector which was fed to the classifiers. Twelve time-domain features were extracted due to their computational simplicity. Also, frequency-domain features were extracted, but with a lower rate, since they are

computationally intensive. Only three frequency-domain features were extracted. Time-domain features are the most popular features in pattern recognition applications which can be calculated in real-time (Angkoon et al., 2009). Mean value, standard deviation (SD), skewness, variance, zero crossing, root mean square, peak, kurtosis, integral of absolute value, simple square integral, mean absolute value, and slope sign change were used to extract features from each time window (Angkoon et al., 2009; Geethanjali & Ray, 2014; Oskoei & Hu, 2008; Riillo et al., 2014; Xi et al., 2017). Mean frequency (MNF), median frequency (MDF) and spectral power magnitude (SPM) were utilized as frequency-domain features to extract useful information from signals' frequencies. Extracted features were normalized in order to eliminate dimensional disparities and scaling. The number of elements in the feature vector (input) is variable and can be calculated using the following equation:

$$Input = 15 \times \text{number of windows} \times \text{number of features} \dots\dots\dots (1)$$

Where 15 is the number of sensors, and the features were extracted from 3000 samples.

The number of windows can be calculated as follows:

$$\begin{aligned} \text{number of windows} &= \frac{\text{number of samples} - \text{window size}}{\text{Delay time}} \dots\dots\dots (2) \\ &= \frac{3000 - \text{window size}}{100} \end{aligned}$$

For instance, for two features and a window of 600 ms size (24 windows) the input can be calculated using equations (1) and (2):

$$Input = 15 \times 24 \times 2 = 720$$

The number of outputs was six classes (each class for each activity), and it was fixed throughout the experiment. Single feature performance test was performed, and features with poor performance were excluded and new feature sets were obtained.

3.8 Pattern recognition algorithms

The classification algorithm plays a vital role in the overall recognition performance, recognition efficiency and computational complexity (Chen & Wang, 2013). In this work, eight of the common pattern recognition multiclass classifiers were evaluated and compared, namely, linear discriminant analysis, decision tree (DT), artificial neural networks, k-nearest neighbors and support vector machine. The optimum classification parameters were chosen based on the performance of the classifier and the complexity of the algorithm. For instance, in the artificial neural networks, increasing the number of neurons would improve the network performance; however, a high number of neurons would lead to slow convergence and training as well as overfitting. Therefore, the optimum classification parameters were selected in order to make a trade-off between the classification performance and algorithm complexity (avoiding overfitting, biased results and slow convergences). MATLAB R2017a libraries and apps were used to extract features and process all the classification algorithms.

3.8.1 Linear discriminant analysis

LDA classifier computes K hyperplanes (linear discriminant functions), where K is greater than 2, and these hyperplanes separate features linearly into different classes (Riillo et al., 2014). The classifier selects the maximum linear discriminant function as the classification rule. All classes have a common covariance matrix while a feature vector is multivariate normally distributed in each class (Chen & Wang, 2013). In this

work, the two types of discriminant analysis (linear discriminant and quadratic discriminant) were tested, which both utilized `fitcdiscr` function, and linear discriminant classifier was selected since it had better performance.

3.8.2 Decision tree

DT classifier is among the most popular classifiers used in approximating discrete-valued functions and inductive inference. It is capable of learning disjunctive expression and is robust when it comes to classifying noisy data. DT is represented as sets of if-then rules in order to improve readability (Polat & Gunes, 2007). DT develops a tree with a root that is split into a number of subsets with internal nodes which contain attribute test conditions, and these subsets are further subdivided until they reach the leaf (Geethanjali & Ray, 2014). In this experiment, the number of leaves was varied from low (maximum number of splits not more than four) to high (maximum number of splits not more than 100). To optimize the decision tree classifier, trial and error method was used to find the optimal number of splits since there is no general rule which can guarantee that the classifier will separate the data optimally, and it was found that 20 was the optimal number of splits.

3.8.3 k-Nearest-Neighbor

k-NN is a classification algorithm that depends on memory. It predicts a class of the test sample based on its k nearest neighbor training sample. Majority vote is used to classify a test sample among the k neighbors. Features need to have zero mean and variance of 1 in order to be measured in the same unit. Euclidean distance is used in feature space to decide which k-neighbor is the nearest to the test sample (Chen & Wang, 2013; Hastie, Tibshirani, & Friedman, 2009). In this study, k was varied from 1 to 100 in order to optimize the classifier. The optimal number was found to be equal to 10 using trial and error method. Furthermore, several distance metrics were evaluated such as

cosine distance, Euclidean distance, and cubic distance. Euclidean distance had the best performance with the k-NN classifier; therefore, it was chosen as the distance metric of the classifier.

3.8.4 Artificial neural network

Artificial neural networks, also called neural networks, are a non-linear classifier which is inspired by the neural networks of a biological brain. A series of weighted nodes, which called neurons, is utilized by ANN to perform information processing (Riillo et al., 2014). These neurons are arranged in three layers, called input layers, hidden layers and output layers, and are interconnected with each other which structure an architecture of the network. In ANN, it is required to make a few choices about the neural network ahead of time to ensure that the network is complex enough to classify the training data. The network should not be too complex that makes training very slow. In this work, for simplicity, one hidden layer was chosen and for optimizing the neural network the number of neurons was ranged between 10 and 100, and cross-validation method was used to choose the optimal number of neurons. It was found that after 20 neurons the classification performance did not improve. The learning rate was set to 0.1 to avoid overfitting and slow convergence. Thus, scaled conjugate gradient backpropagation was implemented as a training function with 20 neurons in each layer (Riillo et al., 2014), and the maximum number of iteration before the training procedure terminated was set to 1000. A sigmoid transfer function was used in the hidden layers which gives a value between 0 and 1, and a softmax transfer function was used for the output layers. Figure 3.14 shows the architecture of ANN of a window of 300 ms size (with a 100 ms overlapping) and two feature. The input layer consisted of 810 (15 sensor x 27 windows x 2 feature) whereas the output layer had 6 neurons wherein each neuron represents a different class (an activity).

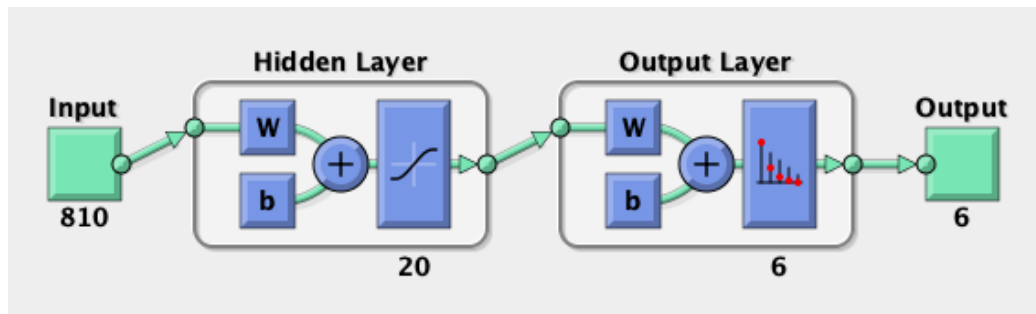


Figure 3.14: Architecture of ANN used to classify six activities using two feature and a window of 300 size

3.8.5 Support Vector Machine

Support vector machine aims to separate data sets using optimal hyperplanes between different classes (Bitzer & Smagt, 2006). SVM is a powerful classification tool which can perform linear classification, and with the usage of kernels, SVM can perform non-linear classification without substantially increasing computational costs. SVM is a binary classifier which means it can be used only to classify two data sets; however, adapted methods can make SVMs a multi-classifier. For instance, one-against-all (OAA) approach uses one SVM per class and trains this SVM to discriminate training samples of a certain class from other training samples of other classes (Oskoei & Hu, 2008). Another approach is one-against-one (OAO) which separates a pair of two classes by training $k(k-1)$ binary classifiers. The class with the greatest number of votes of the $k(k-1)$ classifiers will be chosen as the final output (Wu, Lin, & Weng, 2004).

Kernels are used to develop a complex non-linear classifier. Gaussian and polynomial are among the most popular kernels in the SVM classifier, and it is unclear that which kernel is optimal for this application. Also, there is no one right approach which can be followed to choose the optimal kernel. Therefore, four SVM classifiers were tested using

Gaussian kernel, linear kernel, quadratic kernel, and cubic kernel, and OAO method was adopted to conduct multiclass classification since OAO method resulted in better performance compared to OAA.

3.9 Evaluation

In order to calculate the classification accuracy, the data set was first randomized and, the k-fold cross-validation method was employed for all the classifiers. In the k-fold cross-validation, the dataset was divided into k subsets. Each time one subset was used as the test set while the remaining subsets (k-1) are used as the training set. This holdout method is repeated k times, and k was chosen to be 5. The accuracy results were averaged to get the final classification accuracy. The optimal classifier was tested using 20% of the data set which was held out from the training data set while 80% of the data set was used for training.

To determine the relationship between classification accuracy and window length, classification accuracies were first averaged after that a regression analysis was performed to each classifier. *P*-value was computed, and the threshold of the accepted error was set to 5%. Also, regression analysis was used to determine the impacts of increasing the number of features on classification accuracies.

CHAPTER 4: RESULTS AND DISCUSSION

4.1 Data preprocessing and collection

Three trials of sit-to-stand and stand-to-sit movements with their corresponding ground reaction forces are shown in Figure 4.1 and Figure 4.2. Each movement consisted of 3000 samples (3 seconds), and for the sake of making the figure more readable the x-axis of the figures was displayed in percentage (meaning each 10% is each to 300 samples).

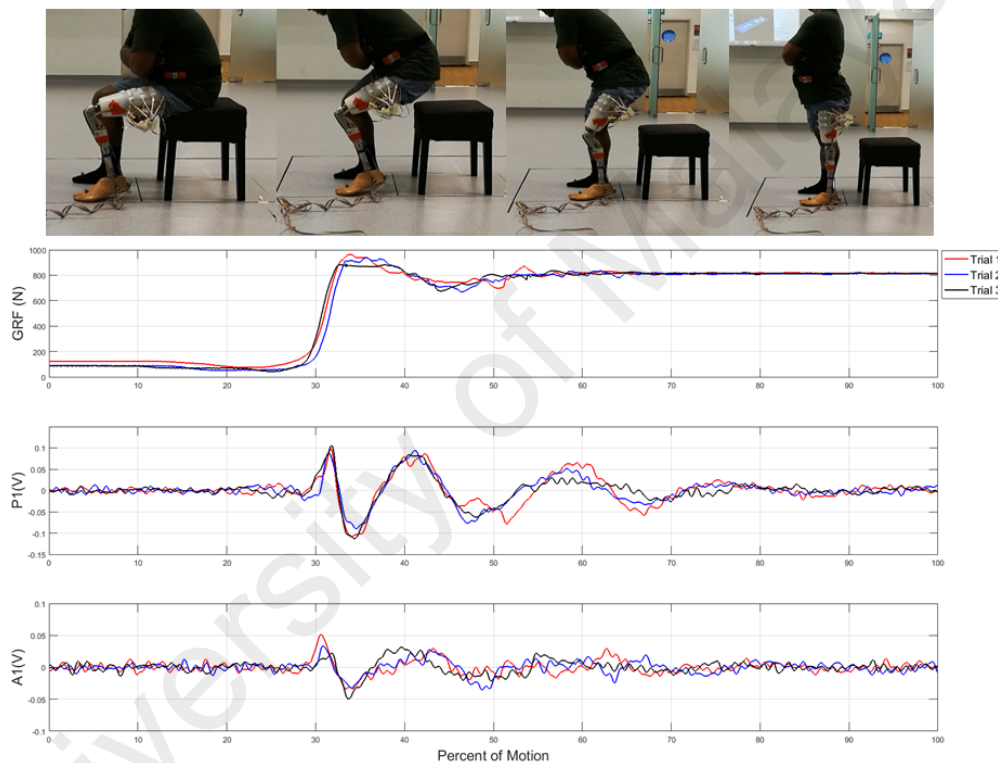


Figure 4.1: Three trials of P1 and A1 signals of sit-to-stand movements with the corresponding GRFs,

The first sensor from the posterior side (P1) and the first sensor from the anterior side (A1) showed the piezoelectric sensors burst at posture transition, which happened when the subject changed his position from sitting position to upright position and vice versa. In the sit-to-stand movement, the ground reaction forces and piezoelectric sensors seemed to be unchanged from 0 to 20%. This was the period where the subject was stationary. After that, the subject starts the first phase of the sit-to-stand movement (trunk flexion), and the signals of the two sensors start oscillating. During trunk flexion phase, the subject

exerted a force on the ground which made the GRFs change. The second phase of sit-to-stand movement (knee extension) depends mostly on the hamstring muscle group; thus, the amplitude of the P1 (0.1 mV) is almost double the amplitude of A1(0.05mV). The last phase was trunk extension that occurred when the subject tried to stabilize his legs at an upright position, as illustrated in Figure 4.1(a) from (55% -80%) (Millington, Myklebust, & Shambes, 1992). At this phase, the subject shifted his body weight in order to balance; therefore, the signals of P1 and A1 oscillated in this phase.

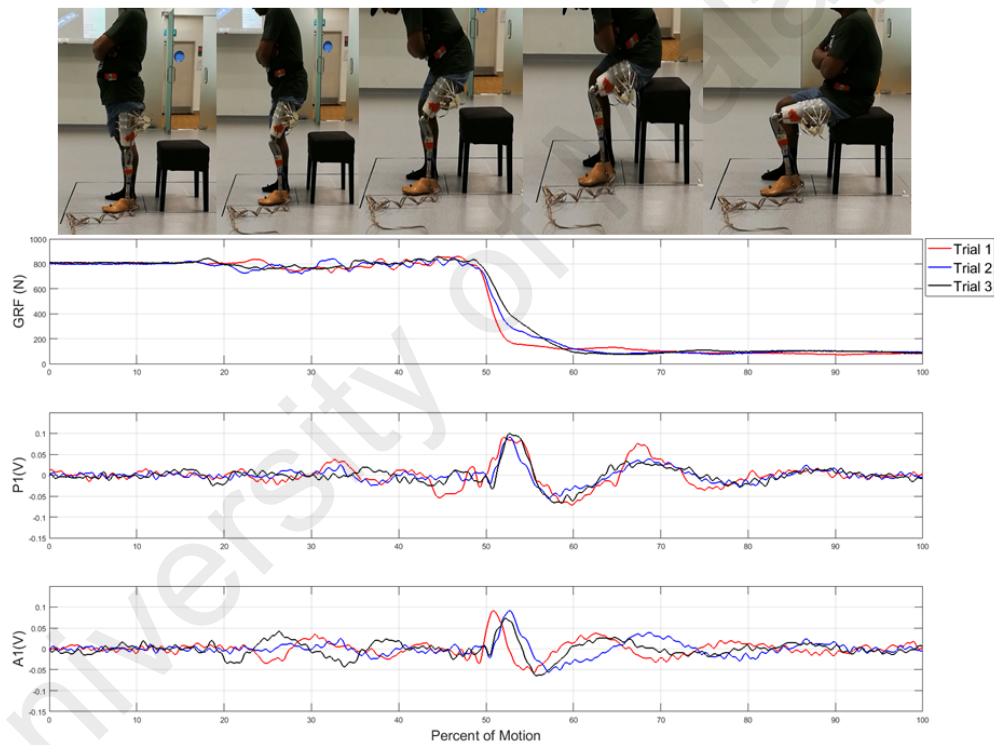
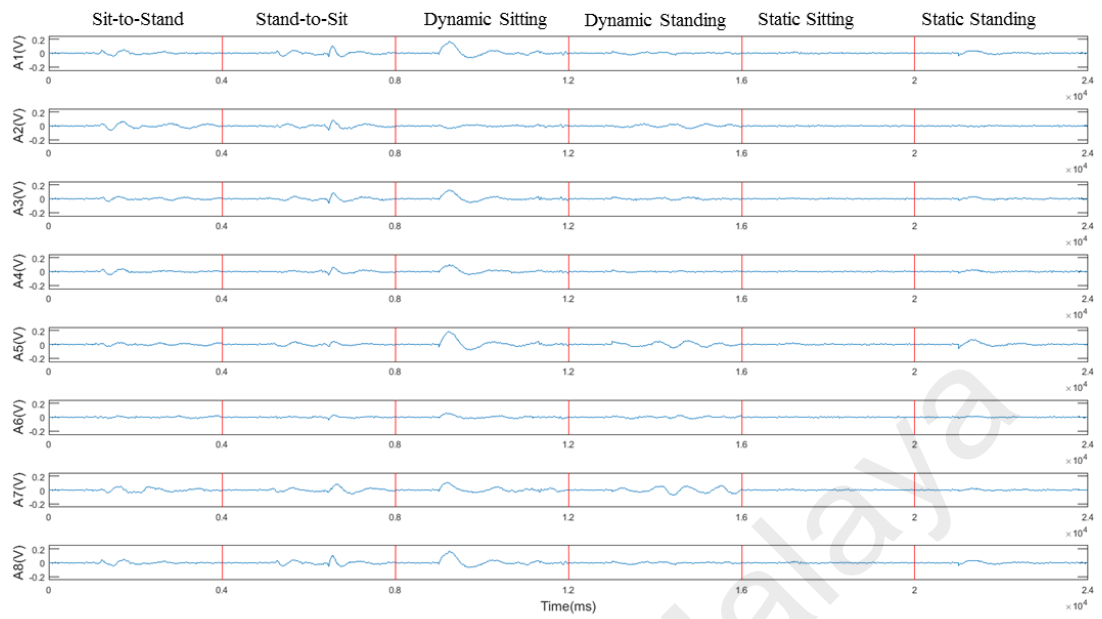
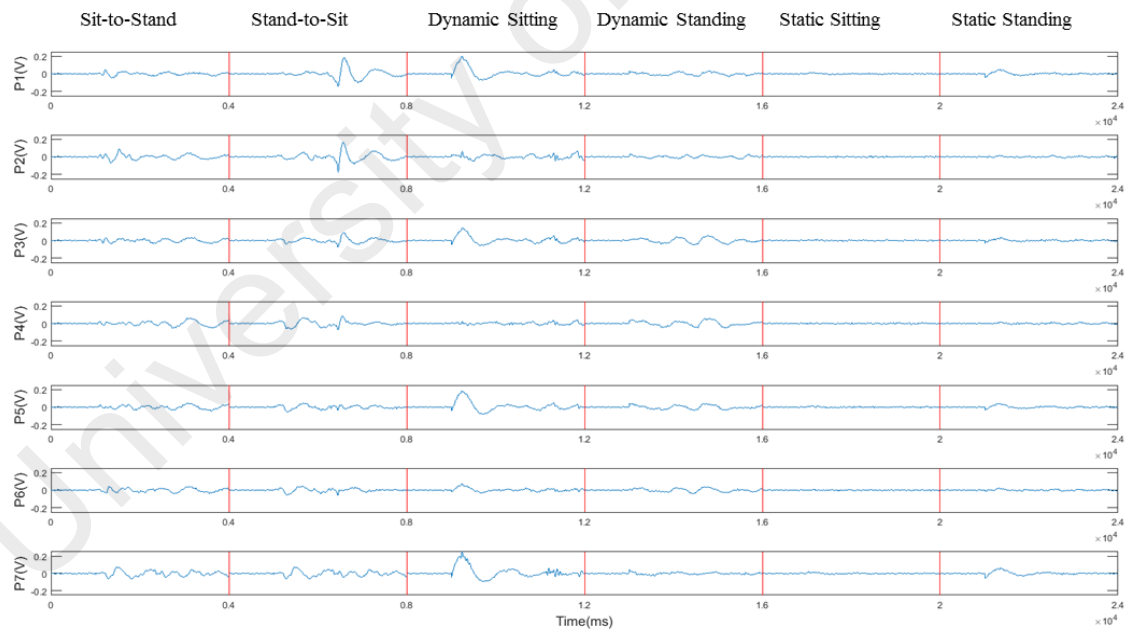


Figure 4.2: Three trials of P1 and A1 signals of stand-to-sit movements with the corresponding GRFs.

Figure 4.2 shows three trials of stand-to-sit movement with their corresponding GRFs, similar to sit-to-stand movement, the piezoelectric signal reaches its peak amplitude at posture transition. At posture transition, both muscle groups quadriceps and hamstrings aided in performing the stand-to-sit movement. For this reason, both sensors P1 and A1 have an amplitude of 0.1 mV.



(a)



(b)

Figure 4.3: The fifteen sensors' filtered and amplified signals of the six different activities (a) the anterior sensors, (b) Posterior sensors

Figure 4.3 (a) and (b) show the piezoelectric signals recorded from the subject, depicting the fifteen sensors filtered and amplified signals of the six different activities. It can be seen from the figures that the signal's pattern generated for each movement is distinguish which makes it easier for the algorithm to extract useful information from the signal (features). The designed signal conditioning circuits, the experimental protocol, the data collection method, and the chosen piezoelectric sensors could obtain a distinguish pattern for each movement. Also, it is obvious that for the stand-to-sit movement the upper sensors for both sides (anterior and posterior) generated higher amplitude than the low sensors which indicates that upper sensors had more important information than the lower sensors. On the other hand, the peak of the dynamic sitting movement fluctuated between 0.05V and 0.2 V in all the sensors, therefore; it was a good decision to cover all the active regions of the quadriceps and hamstring muscle in order to feed the algorithm with all the beneficial information. It can be concluded that the designed signal conditioning circuitry, the developed data acquisition method, and the experimental protocol could generate a pattern with good consistency for the movements. The A1 and P2 sensors generated signals with a high positive correlation which indicates that classifier would easily classify these movements since the pattern is repeated.

4.2 Feature selection results

The feature selection test was performed in two stages. The first stage evaluated single features while the second stage compared selected feature sets.

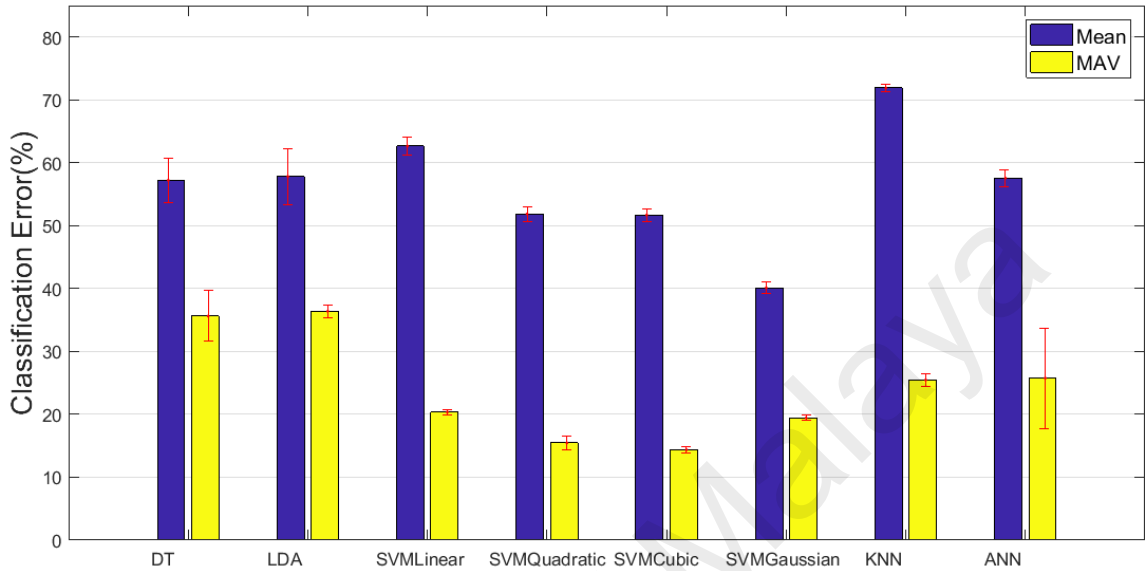


Figure 4.4: Averaged classification errors and standard deviations of Mean and MAV features and their standard deviations with the eight classifiers

Figure 4.4 compares averaged classification errors of two time-domain features (mean value and mean absolute value) and their standard deviations with the eight classifiers are illustrated. Although both features measured the average values of a segmented signal, MAV evaluates only the average of the absolute value of the signal. It can be seen in Figure 4.4 that MAV outperformed Mean, and it had lower classification error values in all classifiers. MAV had its best performance with SVM with cubic kernel with a classification error of less than 15%. On the other hand, the Mean feature had its best classification performance at 40% classification error using SVM with Gaussian kernel. K-NN classifier had the highest classification error (more than 70%), this can be reasoned by that the feature vector (Mean) had a very small range of values which made the classifier unable to distinguish different classes and performed ineffectively.

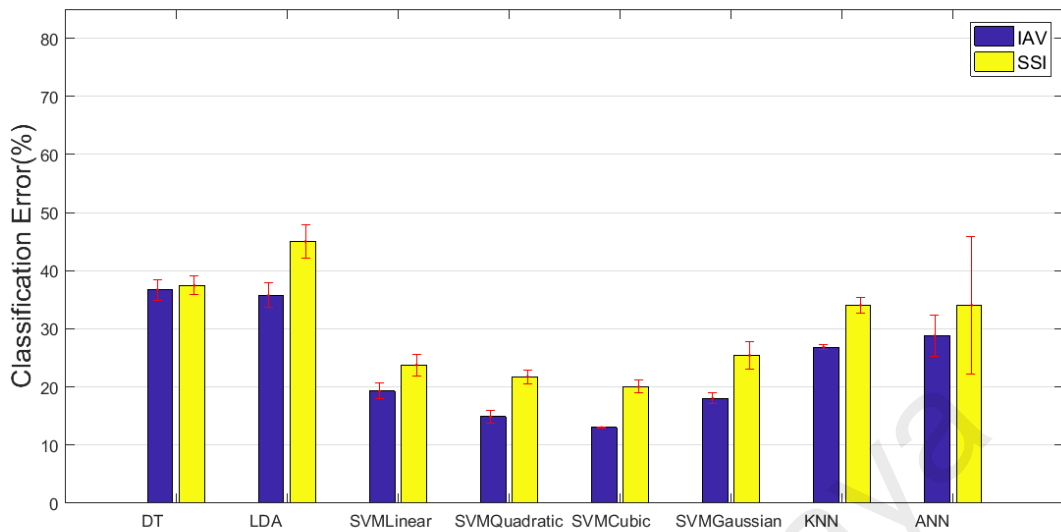


Figure 4.5: Classification errors and standard deviations of IAV and SSI features with the eight classifiers

Figure 4.5 shows the averaged classification errors of eight classifiers with two single time-domain features (integral of absolute value and simple square integral). Also, it illustrates the standard deviation values of these errors. Although both features evaluated the summation of the absolute value of a signal, SSI found the summation of the signal square values. In all the eight classifiers, IAV had lower classification errors compared to SSI. Similar to MAV, IAV and SSI had their best performances with SVM with cubic kernel, approximately 13%, and 20% errors, respectively. However, DT and LDA classifiers could not classify the activities well for both features (IAV and SSI). ANN also failed to successfully distinguish different classes. It can be reasoned by the inadequate number of features which were fed to the classifier since ANN requires either a high training data set or a high number of features in order to perform at its best. Thus, increasing the number of features may result in an improvement of ANN's classification accuracy. Due to the poor performance of ANN, its standard deviation of SSI was higher

than other standard deviations (more than 300%). Also, ANN classifier changes its initial conditions in every new training which generates different results.

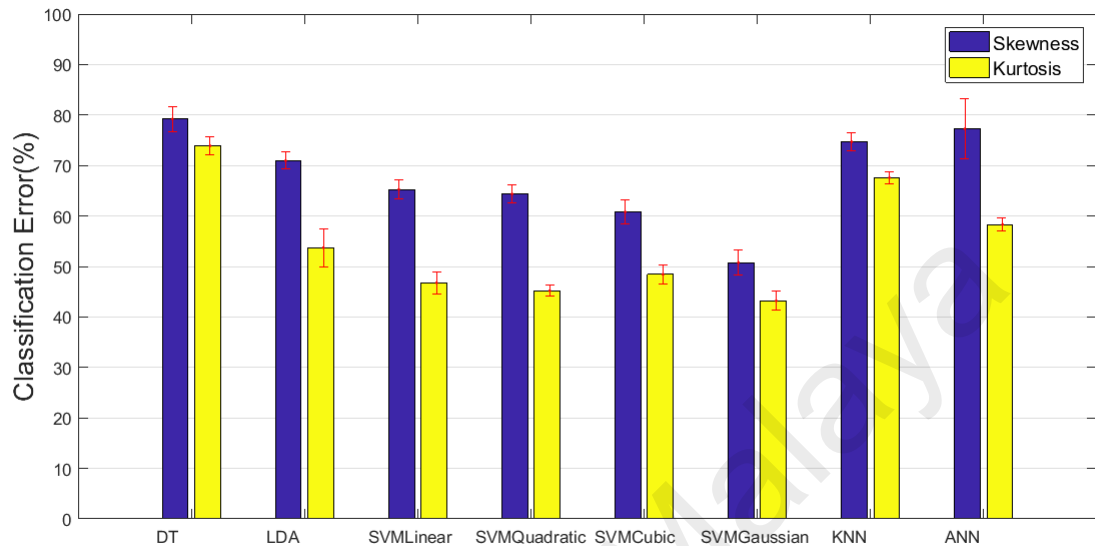


Figure 4.6: Averaged classification errors and standard deviations of Skewness and kurtosis features with the eight classifiers

Both kurtosis and skewness measured how the data were distributed compared to the normal distribution. Kurtosis shows if the tail of the data exceeded the normal distribution tail. On the other hand, skewness measured the asymmetry of data from the normal distribution. Figure 4.6 depicts the averaged classification errors and standard deviations of two time-domain features (kurtosis and skewness) with the eight tested classifiers. These two statistical terms were used as time-domain features to extract useful information from the signal's windows; nonetheless, both features had poor performance, all classification errors were more than 40% in all classifiers. Skewness was not a useful feature since it had a classification error of more than 70% with DT, LDA, KNN, and ANN classifiers.

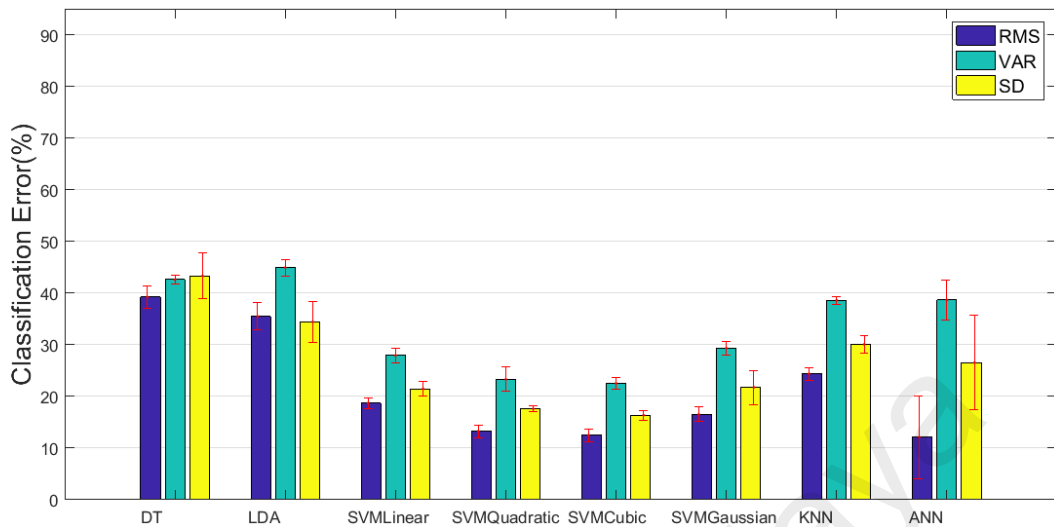


Figure 4.7: Averaged classification errors and standard deviations of RMS, SD, and VAR features with the eight classifiers

SD and VAR were used to measure and quantify the spread and the variation of the segmented signal from its mean. RMS could have the same value of SD if the signal segmented had a zero mean. Figure 4.7 shows the averaged classification errors and their standard deviations of RMS, SD, and VAR with the eight classifiers. RMS had the lowest classification errors among the three features with all the classifiers. SD outperformed VAR in all the classifiers but DT. DT and LDA had poor performances with all the three features this can be explained by the nonlinearity of the features since these classifiers work better with linear feature dataset. SD and VAR had their lowest classification errors (16.37% and 22.53%, respectively) with SVM with cubic kernel classifier whereas RMS lowest classification error was achieved by ANN classifier (12.12%).

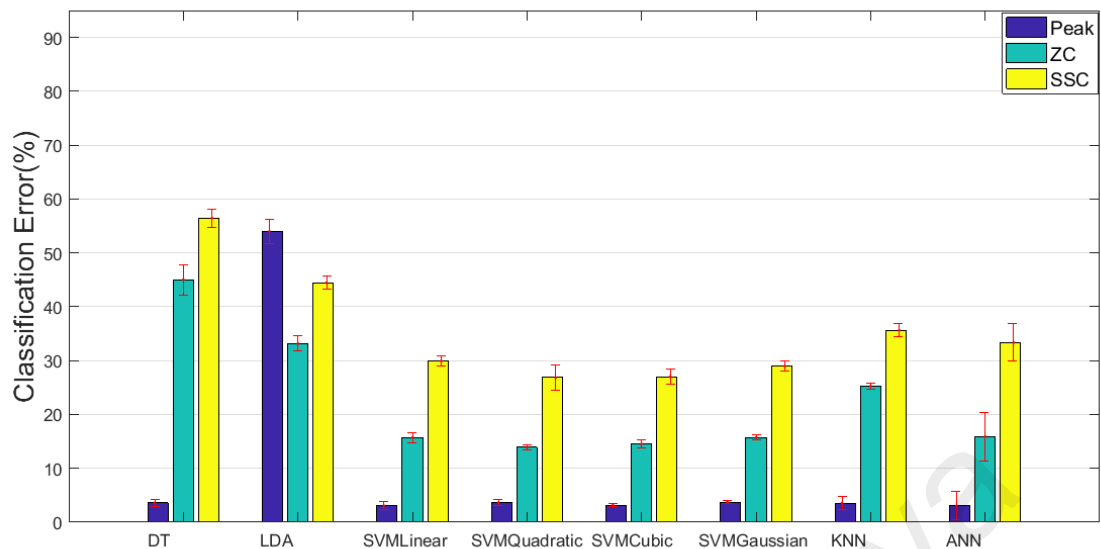


Figure 4.8: Averaged classification errors and standard deviations of Peak, ZC and SSC features with the eight classifiers

Peak number, zero crossing, and slope sign change all described the frequency of the signal but in the time domain. Figure 4.8 shows the classification errors and standard deviations of three time-domain features (Peak, ZC, and SSC) with the eight classifiers. It is obvious that Peak feature was not only the best of the three features compared but the best time-domain feature tested in this thesis since it had the lowest classification errors with all the classifiers but LDA. The lowest classification error of Peak feature was achieved by ANN classifiers (approximately 3%). However, the LDA classifier failed to discriminate the six classes of activities since Peak feature was not linearly distributed which made it difficult for the classifier to create linear hyperplanes to separate the classes. ZC performed well with SVM four classifiers, and its lowest classification error was obtained by SVM with cubic kernel. On the other hand, SSC had classification errors of more than 25% with all the classifiers.

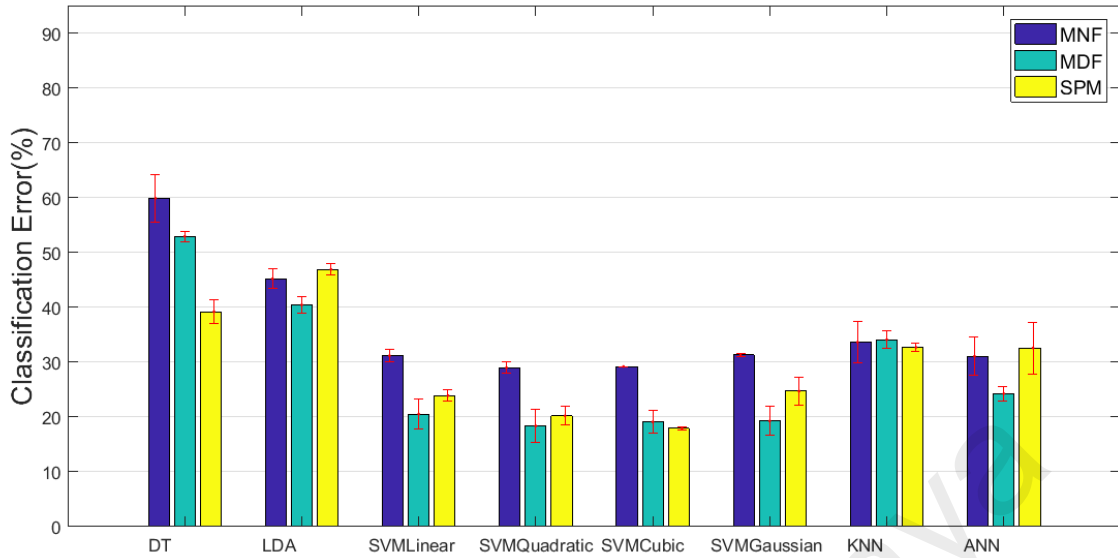


Figure 4.9: Averaged classification errors and standard deviations of MNF, MDF, and SPM features with the eight classifiers

Mean frequency, median frequency, and spectral power magnitude are all frequency-domain features which required a fast Fourier transform for the segmented signal before extracting features. Figure 4.9 depicts the averaged classification errors and their standard deviations of the three frequency-domain features (MNF, MDF, and SPM) with the eight classifiers. MNF had the poorest performances of the three features with most of the classifiers. On the other hand, MDF had the lowest classification errors with LDA, ANN, SVM with linear, quadratic, and Gaussian kernels whereas the rest classifiers performed better with SPM feature. MDF and SPM achieved their lowest classification errors with SVM with cubic kernel 19.10% and 17.93%, respectively.

Table 4.1. shows the classification accuracies, in descending order, of the eight classifiers with the 15 single features extracted from a 300ms sliding window with 100 ms overlapping. Single time-domain features such as skewness, and kurtosis had classification accuracies less than 57% with all the classifiers. On the other hand, single features such as IAV, Peak, RMS, and MAV have better classification accuracy. All the

frequency-domain features had better accuracies with SVM classifiers than with the other classifiers. MDF had the best performance among the frequency-domain features, achieving its classification accuracy with SVM with Quad kernel (81.63%). LDA classifier had its highest classification accuracy using ZC (66.83%) while all the other classifiers achieved their highest classification accuracies using the number of peak feature (Peak).

Table 4.1: Classification accuracies (%) of the 15 single features with the eight classifiers

	DT	LDA	SVM Linear	SVM Quad	SVM Cubic	SVM Gaussian	KNN	ANN
Peak	96.40	46.00	96.93	96.37	96.83	96.27	96.43	96.97
RMS	60.77	64.53	81.30	86.73	87.50	83.47	75.63	87.88
ZC	54.97	66.83	84.27	86.10	85.47	84.27	74.70	84.10
MAV	64.37	63.60	79.63	84.53	85.63	80.57	74.53	74.23
IAV	63.27	64.23	80.70	85.10	86.97	81.93	73.13	71.20
SD	56.67	65.57	78.53	82.40	83.63	78.23	69.93	73.48
MDF	47.07	59.57	79.47	81.63	80.90	80.73	65.90	75.75
SPM	60.80	53.10	76.10	79.77	82.07	75.30	67.30	67.42
SSI	62.53	54.97	76.20	78.23	79.97	74.57	65.93	65.92
VAR	57.40	55.07	72.07	76.70	77.47	70.67	61.40	61.35
SSC	43.53	55.53	70.07	73.13	72.97	71.00	64.37	66.65
MNF	40.13	54.80	68.83	71.00	70.80	68.67	66.37	68.92
Kurtosis	26.10	46.27	53.23	54.80	51.57	56.80	32.40	41.68
Mean	42.77	42.17	37.33	48.13	48.30	59.87	28.10	42.43
Skew	20.80	29.03	34.73	35.63	39.20	49.23	25.30	22.73

* Red color represents low classification accuracies, and yellow color represents moderate classification accuracies while green color represents high classification accuracies.

Table 4.2. shows descriptive statistics (minimum, maximum, mean, standard deviation) of computation times taken to extract features from a 300 ms window (consisting of 300 samples). Each feature was extracted 100 times and the descriptive

statistics were calculated based on this dataset. It can be seen clearly that frequency-domain features took a longer time to be computed compared to time-domain features. For instance, the mean values of calculating frequency-domain features were more than 2.2 ms whereas all the time-domain features required less than 1 ms to be computed. The standard deviations of frequency-domain features were greater compared to the other features which may lead to a lag in a real-time application. For example, the maximum computation times of MNF and MDF were both more than 7 ms, it causes a lag of more than 4ms from their mean computation time. Frequency-domain features required a longer time to compute (at least 400%) compared with time-domain frequency since FFT was applied before extracting the features which also may result in putting a heavier load on the processor.

Table 4.2: Descriptive statistics (mean, standard deviation, minimum and maximum) of features' computation time

Feature	Minimum (ms)	Maximum (ms)	Mean (ms)	Standard deviation (ms)
IAV	0.0064	0.8174	0.0447	0.2089
SSI	0.0051	0.8140	0.0254	0.1102
Mean	0.0214	1.5770	0.0586	0.1723
MAV	0.0150	1.5056	0.0527	0.1823
Peak	0.3304	1.7330	0.9008	0.1546
ZC	0.0115	1.5210	0.0468	0.2030
SSC	0.0210	2.5488	0.0811	0.3009
RMS	0.0257	1.822	0.0517	0.1266
SD	0.0248	1.1792	0.0572	0.1526
VAR	0.0107	1.1348	0.0327	0.1188
Skewness	0.2986	1.8178	0.4813	0.2056
Kurtosis	0.3606	2.1250	0.5203	0.2385
MNF	2.3008	7.2154	3.1374	0.8788
MDF	2.3059	7.9729	3.2552	0.8119
SPM	1.5920	4.0177	2.2330	0.4870

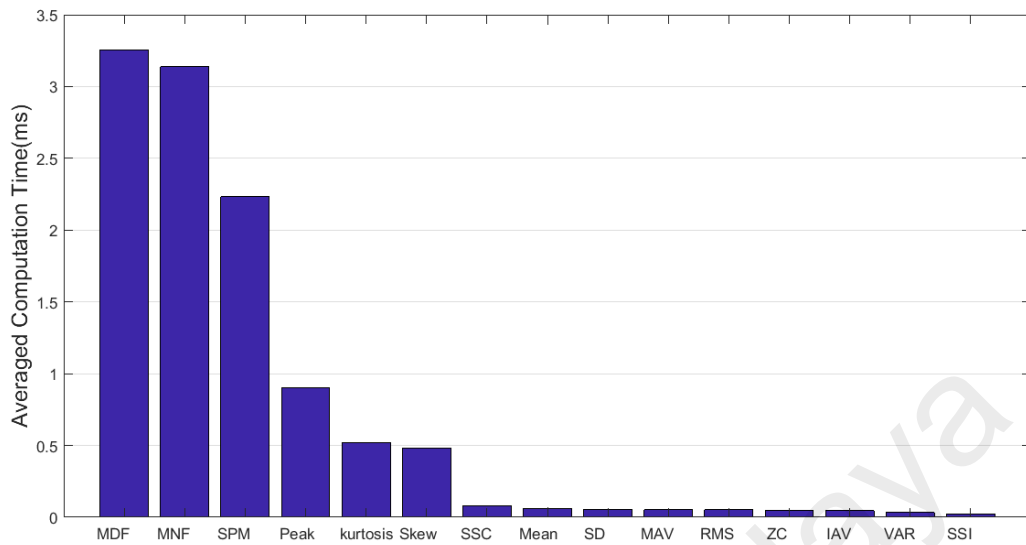


Figure 4.10: Averaged computation time of the single features in descending order

Figure 4.10 shows the mean values of times required to compute each feature in descending order. Three time-domain features (peak, skewness, and kurtosis) had higher means compared to the other time-features. The rest of time-domain features required less than 1 ms to be computed.

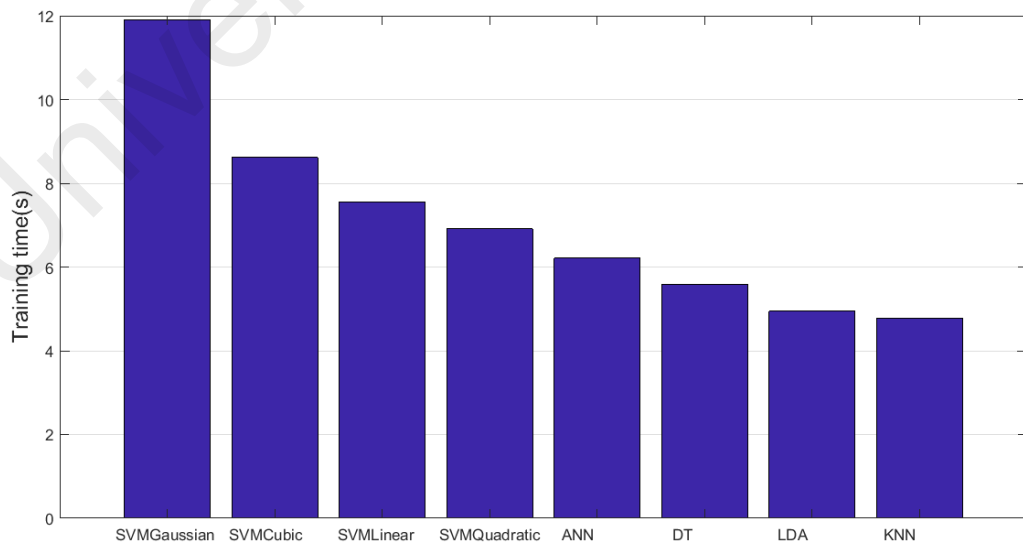


Figure 4.11: Averaged training time of the eight test classifiers

Figure 4.11 shows averaged training times of the classifiers. It can be seen that SVM classifiers had higher training time than the other classifiers. Unlike ANN and LDA, SVM classifiers are non-parametric models which means increasing the training samples would increase the complexity of the model. Although generalized linear models (parametric models) are faster to learn from data, their complexity is limited and constrained to a specific form. It should be mentioned that evaluating classifiers' computational complexity requires sophisticated means such as varying input size and comparing computational recourses (time, memory space) which are out of the scope of this work (Cocco & Monasson, 2001). All the eight classifiers required an average training more than 4 s.

Table 4.3. lists the mean, maximum, minimum and standard deviation of classifiers predication time. It can be seen that SVM with Gaussian kernel had the slowest prediction time while LDA has the fastest. However, all the classifier had prediction speeds of more than 100 observation/second which were quite fast and sufficient for a real-time application.

Table 4.3: Mean, maximum, minimum and standard deviation of the prediction time of the eight classifiers

Classifier	Mean Prediction Time (s)	Max	Min	SD
DT	0.0073	0.0091	0.0063	0.0012
LDA	0.0063	0.0071	0.0050	0.0008
k-NN	0.0071	0.0083	0.0059	0.0010
ANN	0.0076	0.0083	0.0067	0.0007
SVMLinear	0.0075	0.0083	0.0065	0.0006
SVMQuadratic	0.0078	0.0091	0.0067	0.0009
SVMCubic	0.0077	0.0083	0.0071	0.0005
SVMGaussian	0.0082	0.0100	0.0071	0.0011

Due to the poor performance, features such as Skewness, Kurtosis, Mean, MNF, and SSC were excluded from the next stage tests. New feature sets were obtained by grouping single features based on their performance since features with high classification accuracy indicate good separability. Grouping the best performing features (features with good separability) together would improve the classification accuracy since hyperplanes could be used to separate the good separable data even if a dimension of a feature vector is increased. Five new feature sets were created by grouping the best ten features in the first feature set, the best eight features in the second feature set, the best six and the best four features were gathered in separate sets as well, and the last feature set consisting of only two features. The first feature set (10-feature) consists of ten single features (Peak, RMS, ZC, IAV, MAV, SD, MDF, SPM, VAR, and SSI), and the second feature set (8-feature) consists of eight single features (Peak, RMS, ZC, MAV, IAV, SD, MDF, and SPM). The third (6-feature) and the fourth (4-feature) feature sets had six (Peak, RMS, ZC, IAV, MAV and, SD) and four (Peak, RMS, ZC, and MAV) features, respectively. The Number of Peaks and RMS features were selected to obtain the last feature set (2-feature).

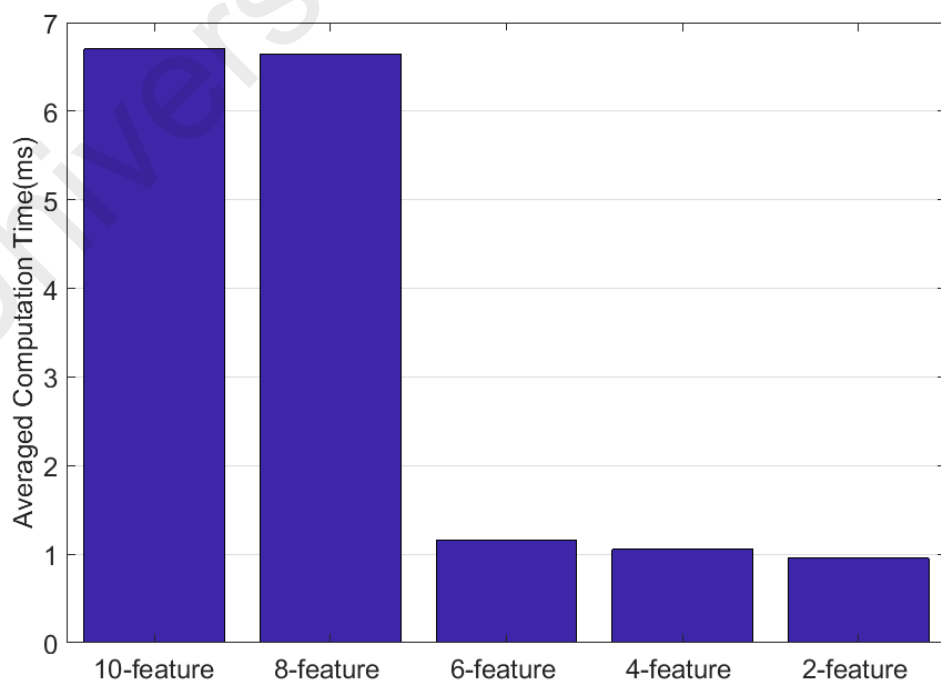


Figure 4.12: The averaged computation time of the obtained five feature sets

Figure 4.12 shows the averaged computation time of the five obtained feature sets. It can be seen that 10-feature and 8-feature sets had substantially higher computation time than the other feature sets due to the computation time of frequency-domain features (SPM and MDF). In contrast, 6-feature, 4-feature, and 2-feature had computation time around 1 ms computation time since all their features were in time-domain. This test was conducted to show how expensive it is to increase the number of features. For instance, increasing the number of features from 2-feature to 4-feature (adding by two features) increased the computation time by approximately 15%. However, by increasing the same number of features (2 features) from 6-feature to 8-feature increased the computation time by almost 440%.

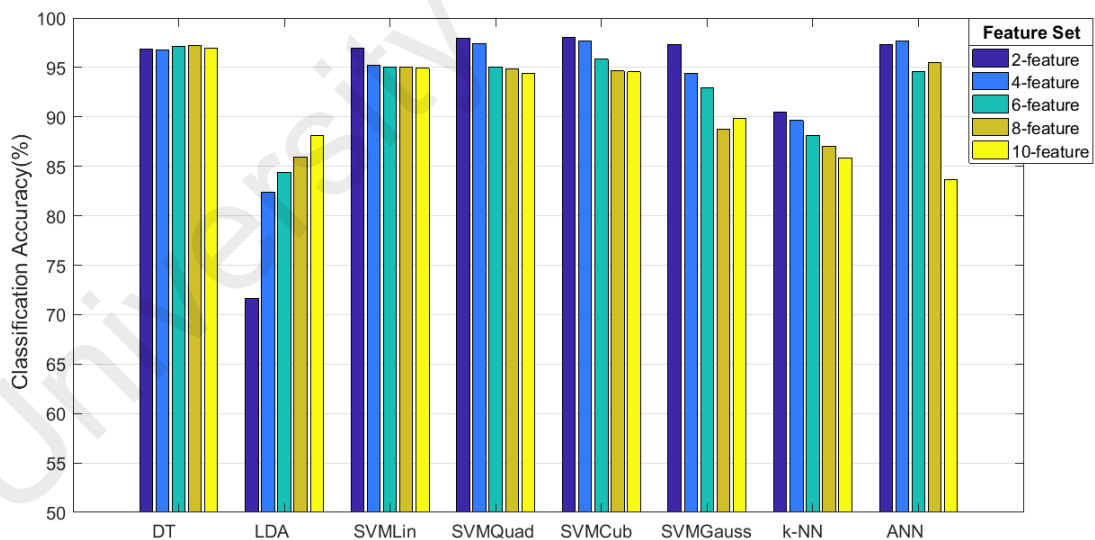


Figure 4.13: Classification accuracy of the eight classifiers with the five obtained feature sets

The classification accuracies of the obtained feature sets are compared in Figure 4.13. The results obtained using feature sets were quite satisfying when compared to the

existing studies. For example, EMG electrodes were used to classify six hand motions of two transradial amputees by ANN and DT using a feature set consisting of MAV, ZC, SSC and waveform length. The obtained averaged accuracies of ANN and DT were 67.90% and 62.50%, respectively (Geethanjali & Ray, 2014). In another study, Mean, RMS and SSC were utilized as a feature vector, extracted from EMG electrodes, to recognize five hand gestures of a transradial amputee. The yielded classification accuracies obtained from SVM, ANN and LDA were all less than 88% (Riillo et al., 2014).

DT, LDA, and ANN had their highest classification accuracies with 8-feature, 10-feature, and 4-feature sets, respectively. On the other hand, k-NN and SVM with linear, quadratic, cubic and Gaussian kernel achieved their highest classification accuracies using 2-feature set. Using only two time-domain features to classify activities will significantly reduce the processing time of controlling a prosthesis which will make it possible to operate in real-time without any substantial delay. The computation time of 2-feature set was less compared to the other feature sets since it had fewer feature numbers. Also, 2-feature set achieved the highest classification accuracy with five classifiers (out of eight) and classification accuracy of more than 95% in six classifiers. Therefore, it can be concluded that 2-feature set (Peak and RMS) outperformed the other feature sets.

Regression analysis was performed to study the relationship between increasing the number of features and the classification accuracies of each classifier. Table 4.4 lists the *P-values* of the test. The results of this section can be summarized as follows: DT and LDA had regression lines with positive slopes (increasing the number of features would increase classification accuracy) whereas the other six classifiers had regression lines with negative slopes (increasing the number of features would decrease classification accuracy). DT, SVM with linear kernel, and ANN had *p-values* of more than 0.05 which

indicated that increasing the number of features had no significant effects on classification accuracies. On the contrary, LDA and other SVM classifiers had p -values of less than 0.05. Thus, it can be deduced that the number of features affected the classification accuracies, and the output results were not obtained by chance. Although all the SVM classifiers had a negative correlation with the number of features (increasing the number of features decreased classification accuracy), LDA had a positive correlation. Therefore, increasing the number of features in LDA improves the classification accuracy and results in an increase in both memory space and computational time.

Table 4.4: The regression analysis P-values to study the relationship between increasing the number of features and the classification accuracy

Classifier	<i>P_Value</i>
DT	0.4073
LDA	0.0380
SVM Linear	0.1257
SVM Quadratic	0.0172
SVM Cubic	0.0081
SVM Gaussian	0.0177
k-NN	0.0001
ANN	0.0989

4.3 Effects of varying window length

In this section, the dependency of the 2-feature set on varied window lengths was investigated by testing the classifiers' accuracy rates. Due to the poor performances of LDA and the negative correlations between K-NN accuracies and the number of features, these two classifiers were excluded from this test. In total, six classifiers were investigated and compared which are shown in Figure 4.14

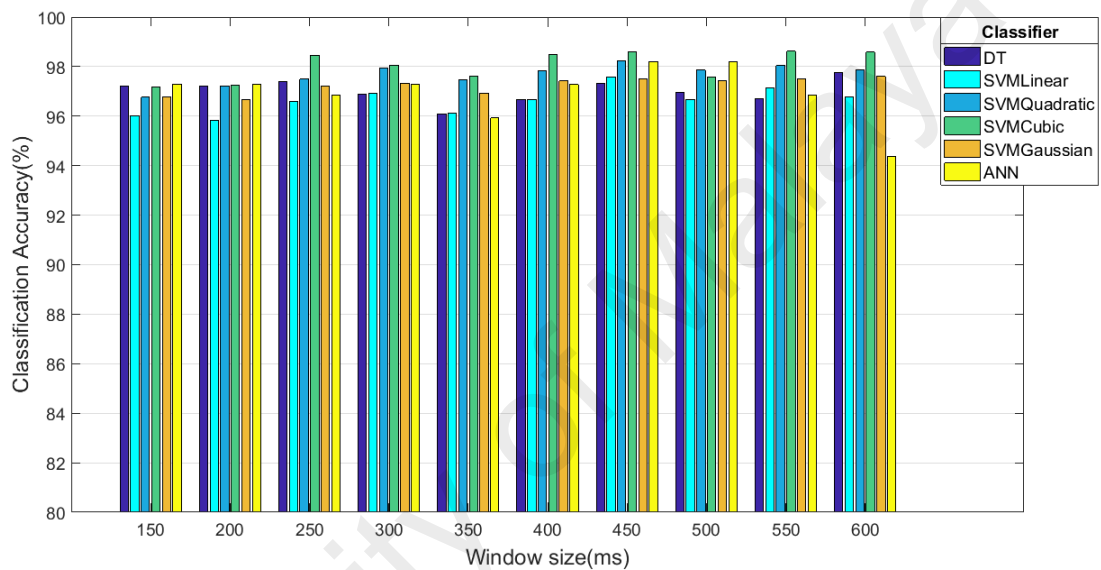


Figure 4.14: The classification accuracies with different. Window sizes (from 150ms to 600 ms)

As it can be seen, most of the classifiers showed no change by increasing the length of a window. The regression analysis showed that varying window lengths from 150ms to 600ms had no significant effect on all the four SVM classifiers ($p < 0.05$). This indicates that for SVM classifiers a small window length could contain enough information to classify different activities of a transfemoral amputee. In contrast, varying window lengths had a significant effect on DT and ANN ($p > 0.05$). It can be clearly seen that varying window sizes affected the classification accuracies of these classifiers. For instance, ANN's accuracy dropped from 98.2 % (in a 400 ms window) to 94.38 % (in a 600 ms window). Table 4.5. lists the p -values of the regression analysis for all classifiers.

The independent parameter was window lengths while the dependent parameters were the classification accuracies of all classifiers.

Table 4.5: The *P-values* of a regression analysis to investigate the impact of window lengths on classifiers' classification accuracies

Classifier	<i>P_Value</i>
DT	0.9158
SVM Linear	0.0430
SVM Quadratic	0.0071
SVM Cubic	0.0225
SVM Gaussian	0.0017
ANN	0.3932

Figure 4.14 shows that windows of size 150 and 200 ms did not have enough information; thus, all the classifiers had classification accuracies almost less than 97%. ANN achieved its highest classification accuracy with 450 and 500 ms windows. Most classifiers attained their best performance at a window of 450 ms. For instance, ANN and SVM with quadratic reached their peaks with accuracies of 98.20% and 98.22%, respectively. SVM with linear kernel had the lowest classification accuracy among the classifiers. It can be concluded that SVM with cubic kernel achieved the highest classification accuracy almost in all the different window sizes (five classifiers more than 98%) including small window sizes indicating they had enough useful information (features).

4.4 Optimal classifier

SVM with cubic kernel was chosen as the optimal classifier because it achieved the highest classification accuracies with almost all window sizes, had no significant effects when the window lengths are varied and had a fast prediction speed. The estimated

medians and confidence interval accuracies of SVM with cubic kernel classifier are shown in the box-plots in Figure 4.15.

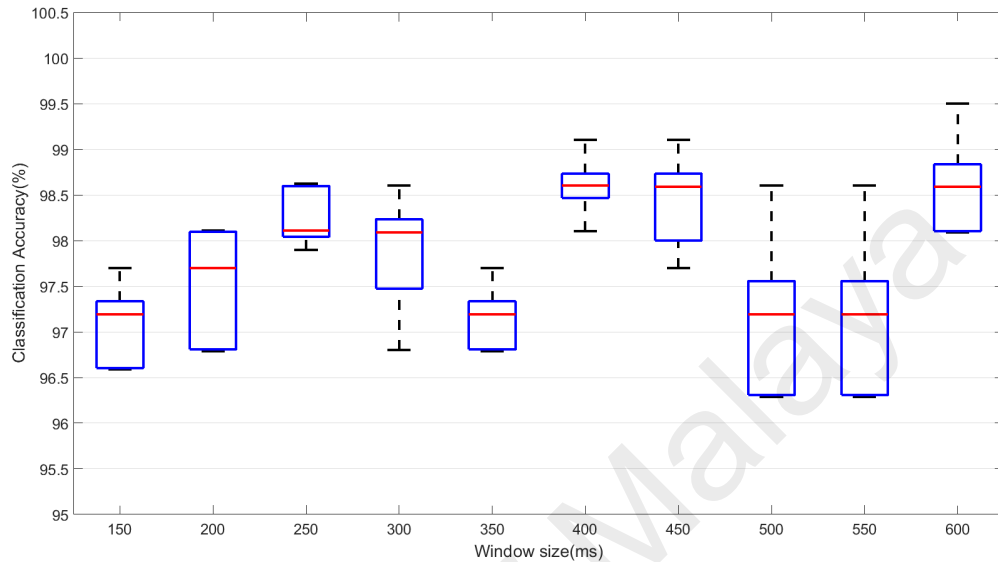


Figure 4.15: Medians and confidence interval accuracies of SVM with cubic kernel

The accuracy ranges of SVM with cubic kernel were narrow in windows of 250, 350 and 400 ms sizes. It is shown in Figure 4.15, for instance, the lowest range was attained by the window of 200 ms size (from 97.9% to 98.62). In contrast, the other windows had wider ranges which may reduce the robustness of a prosthesis's controller. The windows of sizes 500 and 550 ms had the widest range (from 96.29% to 98.6). Real-time controllability requires the window size to be short in order to reduce the processing time. Additionally, it requires the confidence interval of the classifier to be narrow to robustly control the prosthesis. Considering these two factors, it was suggested to choose SVM with cubic kernel with a window of 250 ms size as the optimal classifier's window size since it fulfilled the two requirements.

Table 4.6: Confusion matrix of the testing data set classified by SVM with cubic kernel

		True class					
		Sit-to-stand	Stand-to-sit	Dynamic sitting	Dynamic Standing	Static sitting	Static standing
Predicted class	Sit-to-stand	96.67%	0%	0%	0%	0%	0%
	Stand-to-sit	3.3%	100%	0%	0%	0%	0%
	Dynamic sitting	0%	0%	100%	0%	0%	0%
	Dynamic standing	0%	0%	0%	100%	0%	0%
	Static Sitting	0%	0%	0%	0%	95.00%	1.67%
	Static Standing	0%	0%	0%	0%	5%	98.33%

Table 4.6 shows the confusion matrix of SVM with cubic kernel classifier with the test data set. The testing data set comprised of 20% of the total activities. From the confusion matrix, the overall recognition accuracy was calculated (98.33%) which is quite satisfying. By comparing this accuracy to the existing literature, it is comparable to or even outperforms the previous results. In a study conducted by Hargrove et al. (2013), mechanical sensors and a grid of 96 EMG electrodes were utilized to identify a transfemoral amputee movements such as knee flexion and knee extension the accuracy of the attempted movements was 96% while in this study only 15 piezoelectric sensors yielded a recognition accuracy of 98.33 %. Although most of the activities were correctly predicted, the classifier misclassified some activities such as sit-to-stand as stand-to-sit

and static sitting as static standing. These activities are relatively more difficult to be distinguished due to, probably, the high similarities of each pair's signals.

It can be summarized that the SVM with cubic kernel and 2-feature set was chosen as the optimal classifier since it achieved the highest classification accuracies among all the classifiers with small window sizes (200 – 300 ms). Also, the 250 ms window size was chosen as the optimal window size, and the testing data set was used to evaluate the performance of the optimal classifier with the chosen feature set (2-feature) and the window size (250 ms). The overall recognition accuracy obtained was 98.33%.

4.5 Summary

The designed signal conditioning circuitry, the developed data collection method, and the experimental protocol were able to generate signals which had distinguish patterns for each activity. Having repeated and different patterns for each movement made it easier for the classification algorithms to extract useful features from the sensors' signals.

The feature selection test was performed in two stages. The features were evaluated in the first stage, and selected feature sets were compared in the second stage. Skewness and kurtosis had classification accuracies less than 57% in all the classifiers. In contrast, the number of peaks feature achieved the highest classification accuracy followed by RMS and ZC. All the frequency-domain features attained their best classification performance with SVM classifiers. LDA classifier had its highest classification accuracy using ZC while the other classifiers achieved their highest classification accuracies using peak feature. Some features such as Skewness, Kurtosis, Mean, MNF, and SSC were excluded from the next stage tests due to poor performance. Five new feature sets were obtained by grouping single features based on their performance. DT, LDA, and ANN had their

highest classification accuracies using 8-feature, 10-feature, and 4-feature, respectively. On the other hand, five classifiers (k-NN and SVM with linear, quadratic, cubic and Gaussian kernels) achieved their highest classification accuracies using 2-feature.

The dependency of 2-feature set on varied window lengths was investigated by testing classifiers' accuracy rates. Due to poor performances of LDA and negative correlations between k-NN accuracies and the number of features, these two classifiers were not further tested. SVM with linear kernel had the lowest classification accuracy while SVM with cubic kernel achieved the highest classification accuracy almost in all window lengths. Since SVM with cubic kernel with 2-feature set achieved the highest classification accuracies among all the classifiers and performed better than other classifiers with small window lengths (200 – 300 ms), it was chosen as the optimal classifier. A windows length of 250 ms was chosen as the optimal window since it is suitable for real-time application and had narrow confidence interval. The testing data set was evaluated using SVM with cubic kernel, a window length of 250 ms, and 2-feature set. The overall classification accuracy of the testing data set was 98.33%.

CHAPTER 5: CONCLUSION

This chapter presents a summary of the findings analyzed earlier in the previous chapter. Recommendations for future research and limitations of this study are also detailed in this chapter.

5.1 Summary of the findings

In this thesis, in-socket piezoelectric sensors were used to detect muscle contraction, and signal conditioning circuitry was designed to preprocess sensors' raw data (filtering and amplifying). After that, the data was collected and sampled using data acquisition devices. The experimental protocol, signal conditioning circuits, and the data collection method could generate a repeated and distinguish pattern for each activity.

The next stage was feature extraction, 15 time-domain and frequency-domain features were extracted and then evaluated using eight of the most popular classifiers in pattern recognition. Feature vectors were extracted from a 300 ms sliding window with an overlapping of 100 ms. Features with poor performances were excluded, and the remaining features were combined to obtain five new feature sets. Regression analysis on the number of features and the classifiers showed that the number of features had significant impacts on LDA and SVM with quadratic, cubic and Gaussian kernels. Although the classification accuracies of SVM classifiers were improved by decreasing the number of features, LDA's accuracy decreased by decreasing the number of features. On the other hand, the number of features had insignificant effects on DT, ANN, and SVM with linear kernel. Most of the classifiers yielded their best recognition accuracy with the 2-feature set (RMS and Peak), and SVM with cubic kernel outperformed the other tested classifiers.

Furthermore, the regression analysis on window length and classifiers yielded that DT and ANN had significant effects when the length of a window was varied while all the SVM classifiers had no substantial impacts by varying the length of windows. Additionally, the box-plot of SVM with cubic kernel and the different length windows showed that a 250 ms window had the narrowest accuracy range; thus, it was selected as the optimal window length to ensure robot controllability. The optimal classifier (SVM with cubic kernel) and the optimal window size (250 ms) were tested using a test data set, and the overall recognition accuracy obtained was 98.33%. By comparing this accuracy to the existing literature, it is comparable to or even outperforms the previous results. In a study conducted by Hargrove et al. (2013), mechanical sensors and a grid of 96 EMG electrodes were utilized to identify movements of a single subject (transfemoral amputee). The results showed that using EMG signals improved control of a prosthesis, and classification accuracy of 96% was achieved; however, in this work, 15 piezoelectric sensors were utilized without mechanical sensors and an accuracy of 98.33% was achieved.

Summarizing the findings of the study can conclude that the main outcomes of this study are:

1. This study offered a complete guideline to build signal conditioning circuitry, develop a data collection method for in-socket piezoelectric sensors and an experimental protocol for sitting and standing variation. This work is the first that utilized piezoelectric sensors embedded in the transfemoral socket to perform sitting and standing classification.
2. This study showed a thorough time-domain and frequency-domain feature evaluation and suggested a feature set consisting of only two time-domain

features as the optimal feature set which can be extracted in less than 1 ms and yields high classification accuracy.

3. This study investigated the effect of varying window length on the classification accuracy of different multiclass classification algorithms and suggested an optimal window length (250 ms) which can be utilized for real-time applications.
4. In this study, eight of the most common multiclass classifiers were evaluated to classify six variations of sitting and standing activities, and an optimal classifier was determined (SVM with cubic kernel).

5.2 Limitations of the study

Due to the specificity of individual anatomy, the study was performed on a single subject to establish the classification reliability. Transfemoral amputees have very high variation ratios of muscles' activities during locomotion (including hamstring and quadriceps) (Wentink et al., 2013). Additionally, in a study conducted by Hong and Mun (2005), it was found that variation in measurements of interface pressure between sockets and residual limbs of two transfemoral amputees was large. It can be deduced that performing the experiment on several subjects requires different socket configurations. Also, large variations may result in signal intensity and pattern, which would affect classification results. Therefore, an individual experiment has to be conducted to determine each person's movement classifier based on the same principles.

The practical day to day application may involve hands function to support the body during standing up and sitting down, and this may result in less signal magnitude or even slight variation in the signal responses. Also, practical daily activities involve different body postures with non-central body weight distribution during sitting and standing movements which may yield variations in signal pattern.

The result findings of this study were based on components and instruments described in sections 3.1 and 3.3. If they were changed, the result findings might change as well. This study did not investigate the effects of varying the experiment's components on the result findings.

5.3 Recommendations for future work

This study pioneered the implementation of piezoelectric sensors for transfemoral prostheses-based applications. The study has provided promising results. Nonetheless, it is recommended that further studies expand and validate this work as there were some limitations due to the lack of previous work done using piezoelectric sensors in the fields of pattern recognition and transfemoral development.

Further studies are required to determine the classification performance and its consistency in different subjects with different amputation levels and stump types and thus slightly different sensor-to-muscle configuration. Furthermore, conducting a study with different body postures during sitting and standing with the support of amputee's hands are recommended to expand this work. Also, conducting a real-time experiment consisting of a motorized prosthesis leg and a control law is recommended to expand this work.

Furthermore, detecting the user's intention for movements such as sit-to-stand and stand-to-sit would make their mobility very close to a normal subject. Therefore, it is suggested to conduct a study to investigate the possibility of implementing an intention detection system using piezoelectric sensors and pattern recognition technique.

Overall, the achieved results of this work significantly show improvements over the work of predecessors, and it is believed that piezoelectric sensors may lead to an expansion of practical applications in the field of transfemoral prostheses.

REFERENCES

- Ali, S., Abu Osman, N. A., Eshraghi, A., Gholizadeh, H., bin Abd Razak, N. A., & Abas, W. A. B. (2013). Interface pressure in transtibial socket during ascent and descent on stairs and its effect on patient satisfaction. *Clinical Biomechanics*, 28(9-10), 994-999.
- Angkoon, P., Chusak, L., & Pornchai, P. (2009). A novel feature extraction for robust EMG pattern recognition. *Journal of medical engineering & technology*, 40 4, 149-154.
- B. Hudgins, P. A. P., and R. Scott. (1993). A new strategy for multifunction myoelectric control. *IEEE Trans Biomed Eng*, 40(1), 82-94.
- Ballas, R. G., Schlaak, H. F., & Schmid, A. J. (2006). The constituent equations of piezoelectric multilayer bending actuators in closed analytical form and experimental results. *Sensors and Actuators a-Physical*, 130, 91-98.
- Bitzer, & Smagt. (2006). Learning EMG control of a robotic hand: Towards active prostheses 2006. *IEEE International Conference on Robotics and Automation* (pp. 2819).
- Brooker, G. (2012). *Introduction to biomechatronics*: Scitech Pub Incorporated.
- Chen, & Wang. (2013). Pattern recognition of number gestures based on a wireless surface EMG system. *Biomedical Signal Processing and Control*, 8(2), 184-192.
- Chen, X. P., Zhu, X. Y., & Zhang, D. G. (2010). A discriminant bispectrum feature for surface electromyogram signal classification. *Medical Engineering & Physics*, 32(2), 126-135.
- Cocco, S., & Monasson, R. (2001). Statistical physics analysis of the computational complexity of solving random satisfiability problems using backtrack algorithms. *European Physical Journal B*, 22(4), 505-531.
- Dawley, J. A., Fite, K. B., Fulk, G. D., & Ieee. (2013). EMG control of a bionic knee prosthesis: exploiting muscle co-contractions for improved locomotor function 2013. *IEEE 13th International Conference on Rehabilitation Robotics*.
- Deepa, Thangaraj, & Chitra. (2010). Investigating the performance improvement by sampling techniques in EEG data. *International Journal on Computer Science and Engineering*, 2, 2025-2028.
- Demura, S., & Yamada, T. (2007). Height of chair seat and movement characteristics in sit-to-stand by young and elderly adults. *Perceptual and Motor Skills*, 104(1), 21-31.
- El-Sayed. (2015). Design of knee joint mechanism and in-socket sensor for transfemoral amputees. *University of Malaya*.
- El-Sayed, Abo-Ismael, El-Melegy, Hamzaid, & Abu Osman. (2013). A Development of a Micro-Gripper Using Piezoelectric Bimorphs. *Sensors*, 13(5), 5826-5840.

- El-Sayed, Hamzaid, & Abu Osman. (2014a). Piezoelectric bimorphs' characteristics as in-socket sensors for transfemoral amputees. *Sensors*, 14(12), 23724-23741.
- El-Sayed, Hamzaid, & Abu Osman. (2014b). Technology efficacy in active prosthetic knees for transfemoral amputees: a quantitative evaluation. *Scientific World Journal*.
- El-Sayed, Hamzaid, Tan, & Abu Osman. (2015). Detection of prosthetic knee movement phases via in-socket Sensors: A feasibility study. *The Scientific World Journal*, 13.
- Englehart, K., & Hudgins, B. (2003). A robust, real-time control scheme for multifunction myoelectric control. *IEEE Transactions on Biomedical Engineering*, 50(7), 848-854.
- Eshraghi, A., Abu Osman, N. A., Gholizadeh, H., Ali, S., Saevarsson, S. K., & Abas, W. A. W. (2013). An experimental study of the interface pressure profile during level walking of a new suspension system for lower limb amputees. *Clinical Biomechanics*, 28(1), 55-60.
- Galli, M., Crivellini, M., Sibella, F., Montesano, A., Bertocco, P., & Parisio, C. (2000). Sit-to-stand movement analysis in obese subjects. *International Journal of Obesity*, 24(11), 1488-1492.
- Geethanjali, P., & Ray, K. K. (2014). EMG based man-machine interaction-A pattern recognition research platform. *Robotics and Autonomous Systems*, 62(6), 864-870.
- Hargrove, L. J., Simon, A. M., Young, A. J., Lipschutz, R. D., Finucane, S. B., Smith, D. G., & Kuiken, T. A. (2013). Robotic leg control with emg decoding in an amputee with nerve transfers. *New England Journal of Medicine*, 369(13), 1237-1242.
- Hastie, T., Tibshirani, R., & Friedman, J. (2009). *The elements of statistical learning: data mining, inference and prediction* (2 ed.). New York,: Springer.
- Herr, H., & Wilkenfeld, A. (2003). User-adaptive control of a magnetorheological prosthetic knee. *Industrial Robot-an International Journal*, 30(1), 42-55.
- Hesse, S., Schauer, M., Malezic, M., Jahnke, M., & Mauritz, K. H. (1994). Quantitative-analysis of rising from a chair in healthy and hemiparetic subjects. *Scandinavian Journal of Rehabilitation Medicine*, 26(3), 161-166.
- Hong, J. H., & Mun, M. S. (2005). Relationship between socket pressure and EMG of two muscles in trans-femoral stumps during gait. *Prosthetics and Orthotics International*, 29(1), 59-72.
- Huang, Englehart, Hudgins, & Chan. (2005). A Gaussian mixture model based classification scheme for myoelectric control of powered upper limb prostheses. *IEEE Transactions on Biomedical Engineering*, 52(11), 1801-1811.

- Huang, Kuiken, & Lipschutz. (2009). A strategy for identifying locomotion modes using surface electromyography. *IEEE Transactions on Biomedical Engineering*, 56(1), 65-73.
- Hudgins., B., Parker., P., & Scott., R. N. (1991). The recognition of myoelectric patterns for prosthetic limb control. *Proceedings of the Annual International Conference of the IEEE Engineering in Medicine and Biology Society Volume 13: 1991* (pp. 2040-2041).
- Jasni, F., Hamzaid, N. A., Abd Muthalif, A. G., Zakaria, Z., Shasmin, H. N., & Ng, S. C. (2016). In-socket sensory system for transfemoral amputees using piezoelectric sensors: an efficacy study. *IEEE-ASME Transactions on Mechatronics*, 21(5), 2466-2476.
- Jay Martin, B., CP, LP, Andrew Pollock, BS, Jessica Hettinger, BS. (2010). Microprocessor lower limb prosthetics: review of current state of the art. *American Academy of Orthotists and Prosthetists*, 22(2010), 183-193.
- Kapti, A. O., & Yucenur, M. S. (2006). Design and control of an active artificial knee joint. *Mechanism and Machine Theory*, 41(12), 1477-1485.
- Khatwani, P., & Tiwari, A. (2013). A survey on different noise removal techniques of EEG signals. *International Journal of Advanced Research in Computer and Communication Engineering*, 2(2), 1091-1095.
- Khokhar, Z. O., Xiao, Z. G., & Menon, C. (2010). Surface EMG pattern recognition for real-time control of a wrist exoskeleton. *Biomedical Engineering Online*, 9.
- Kotake T, Dohi N, Kajiwara T, Sumi N, Koyama Y, & T., M. (1993). An analysis of sit-to-stand movements. *Arch Phys Med Rehabil*, 74(10), 1095-1099.
- Kralj, A., Jaeger, R. J., & Munih, M. (1990). Analysis of standing up and sitting down in humans - definitions and normative data presentation. *Journal of Biomechanics*, 23(11), 1123-1138.
- Li, N., Yang, D. P., Jiang, L., Liu, H., & Cai, H. G. (2012). Combined use of FSR sensor array and SVM classifier for finger motion recognition based on pressure distribution map. *Journal of Bionic Engineering*, 9(1), 39-47.
- Lihong Zheng, & Xiangjian He. (2007). Classification techniques in pattern recognition. *Paper presented at the WSCG'2005, Plzen, Czech Republic*.
- Liu, J. W., He, J. Y., Sheng, X. J., Zhang, D. G., Zhu, X. Y., & Ieee. (2013). A new feature extraction method based on autoregressive power spectrum for improving sEMG classification. *2013 35th Annual International Conference of the Ieee Engineering in Medicine and Biology Society* (pp. 5746-5749).
- Lorenzelli, L., Sordo, G., Bagolini, A., & Resta, G. (2017). *Socketmaster: Integrated sensors system for the optimised design of prosthetic socket for above knee amputees*.

- Martinez-Villalpando, E. C., & Herr, H. (2009). Agonist-antagonist active knee prosthesis: A preliminary study in level-ground walking. *Journal of Rehabilitation Research and Development*, 46(3), 361-373.
- Martinez-Villalpando, E. C., Weber, J., Elliott, G., Herr, H. (2008). Design of an agonist-antagonist active knee prosthesis. *2008 2nd IEEE Ras & Embs International Conference on Biomedical Robotics and Biomechatronics* (pp. 529). New York: IEEE.
- Maurizio, R., Matteo, N., Leandro, L., & Davide, B. (2017). *Dual Mode Pressure Sensing for Lower-Limb Prosthetic Interface*. Paper presented at the EuroSensors 2017 Conference, Paris, France,.
- Millington, P. J., Myklebust, B. M., & Shambes, G. M. (1992). Biomechanical analysis of the sit-to-stand motion in elderly persons. *Archives of Physical Medicine and Rehabilitation*, 73(7), 609-617.
- OrtoPed. (2011). Total Knee® 2000 In T. K. 2000 & P. Knee (Eds.), (pp. Prosthetics lower extremity). USA: OrtoPed.
- Oskoei, M. A., & Hu, H. S. (2008). Support vector machine-based classification scheme for myoelectric control applied to upper limb. *Ieee Transactions on Biomedical Engineering*, 55(8), 1956-1965.
- Össur. (2018). Dynamic Solutions. USA: Össur.
- Ottobock. (2016a). C-Leg. In C.-C.-L.-I. f. u. q. p.-E. 3C98-3 (Ed.). Germany: ottobock.
- ottobock. (2016b). Lightweight Hydraulic Knee,<330lbs<150KG. In R. 3R95 (Ed.), *ottobock, lower limb prosthetics knee*. Germny.
- Ottobock. (2017). Single axis knee joint, brake titan. In B. T. Single Axis Knee Joint (Ed.). Germany.
- Park, E. S., Park, C., Lee, H. J., Kim, D. Y., Lee, D. S., & Cho, S. R. (2003). The characteristics of sit-to-stand transfer in young children with spastic cerebral palsy based on kinematic and kinetic data. *Gait & Posture*, 17(1), 43-49.
- PnOCare. (2012). Transfemoral & knee disarticulation. USA: P&O Care
- Polat, K., & Gunes, S. (2007). Classification of epileptiform EEG using a hybrid system based on decision tree classifier and fast Fourier transform. *Applied Mathematics and Computation*, 187(2), 1017-1026.
- Popovic, D., Tomovic, R., Tepavac, D., & Schwirtlich, L. (1991). Control aspects of active above-knee prosthesis. *International Journal of Man-Machine Studies*, 35(6), 751-767.

- Prendergast, Helm, & Duda. (2005). *Analysis of muscle and joint loads. Basic Orthopaedic Biomechanics and Mechano-Biology 3rd edition*, by C Mow and Rik Huiskes (3rd editio ed.). Philadelphia: C. Mow, R. Huiskes.
- Riillo, F., Quitadamo, L. R., Cavrini, F., Gruppioni, E., Pinto, C. A., Pasto, N. C., . . . Saggio, G. (2014). Optimization of EMG-based hand gesture recognition: Supervised vs. unsupervised data preprocessing on healthy subjects and transradial amputees. *Biomedical Signal Processing and Control*, 14, 117-125.
- Roebroeck, M. E., Doorenbosch, C. A. M., Harlaar, J., Jacobs, R., & Lankhorst, G. J. (1994). Biomechanics and muscular-activity during sit-to-stand transfer. *Clinical Biomechanics*, 9(4), 235-244.
- Rouse, E. J., Mooney, L. M., & Herr, H. M. (2014). Clutchable series-elastic actuator: Implications for prosthetic knee design. *International Journal of Robotics Research*, 33(13), 1611-1625.
- Smith, L. H., Hargrove, L. J., Lock, B. A., & Kuiken, T. A. (2011). Determining the optimal window length for pattern recognition-based myoelectric control: balancing the competing effects of classification error and controller delay. *IEEE Transactions on Neural Systems and Rehabilitation Engineering*, 19(2), 186-192.
- Sup, F., Varol, H. A., Mitchell, J., Withrow, T. J., & Goldfarb, M. (2009). Preliminary evaluations of a self-contained anthropomorphic transfemoral prosthesis. *Ieee-Asme Transactions on Mechatronics*, 14(6), 667-676.
- Syrseloudis, Emiris, Maganaris, & Lilas. (2008). Design framework for a simple robotic ankle evaluation and rehabilitation device. *2008 30th Annual International Conference of the Ieee Engineering in Medicine and Biology Society, Vols 1-8* (pp. 4310).
- Thongpanja, S., Phinyomark, A., Phukpattaranont, P., & Limsakul, C. (2013). Mean and median frequency of emg signal to determine muscle force based on time-dependent power spectrum. *Elektronika Ir Elektrotechnika*, 19(3), 51-56.
- Tsukahara, A., Kawanishi, R., Hasegawa, Y., & Sankai, Y. (2010). Sit-to-stand and stand-to-sit transfer support for complete paraplegic patients with robot suit hal. *Advanced Robotics*, 24(11), 1615-1638.
- Vanderbilt. (2013). Prosthetic limb advances could help victims of the Boston Marathon bombings *bionic leg*. USA: Vanderbilt.
- Wang, B., Xie, H., Cong, D., & Xu, X. (2007). Biped robot control strategy and open-closed-loop iterative learning control. *Frontiers of Electrical and Electronic Engineering in China*, 2(1), 104-107.
- Wang, H., Simpson, K. J., Chamnongkich, S., Kinsey, T., & Mahoney, O. M. (2005). A biomechanical comparison between the single-axis and multi-axis total knee arthroplasty systems for the stand-to-sit movement. *Clinical Biomechanics*, 20(4), 428-433.

- Waters RL, Perry J, Antonelli D, & H., H. (1976). Energy cost of walking of amputees: the influence of level of amputation. *J Bone Joint Surg Am*, 58, 6-42.
- Wentink, E. C., Beijen, S. I., Hermens, H. J., Rietman, J. S., & Veltink, P. H. (2013). Intention detection of gait initiation using EMG and kinematic data. *Gait & Posture*, 37(2), 223-228.
- Wheeler, J., Woodward, C., Ucovich, R. L., Perry, J., & Walker, J. M. (1985). Rising from a chair - influence of age and chair design. *Physical Therapy*, 65(1), 22-26.
- Wolf, E. J., Everding, V. Q., Linberg, A. L., Schnall, B. L., Czerniecki, J. M., & Gambel, J. M. (2012). Assessment of transfemoral amputees using C-Leg and Power Knee for ascending and descending inclines and steps. *Journal of Rehabilitation Research and Development*, 49(6), 831-842.
- Wu, Lin, & Weng. (2004). Probability estimates for multi-class classification by pairwise coupling. *The Journal of Machine Learning Research*, 5, 12/1/2004, 975-1005.
- Wu, S. K., Waycaster, G., & Shen, X. R. (2011). Electromyography-based control of active above-knee prostheses. *Control Engineering Practice*, 19(8), 875-882.
- Xi, X. G., Tang, M. Y., Miran, S. M., & Luo, Z. Z. (2017). Evaluation of feature extraction and recognition for activity monitoring and fall detection based on wearable sEMG sensors. *Sensors*, 17(6).
- Yoshioka, S., Nagano, A., Hay, D. C., & Fukashiro, S. (2009a). Biomechanical analysis of the relation between movement time and joint moment development during a sit-to-stand task. *Biomedical Engineering Online*, 8.
- Yoshioka, S., Nagano, A., Hay, D. C., & Fukashiro, S. (2009b). Biomechanical analysis of the relation between movement time and joint moment development during a sit-to-stand task. *Biomedical Engineering Online*, 8, 9.
- Yuan, K. B., Wang, Q. N., & Wang, L. (2015). Fuzzy-logic-based terrain identification with multisensor fusion for transtibial amputees. *IEEE-ASME Transactions on Mechatronics*, 20(2), 618-630.
- Zijlstra, A., Mancini, M., Lindemann, U., Chiari, L., & Zijlstra, W. (2012). Sit-stand and stand-sit transitions in older adults and patients with Parkinson's disease: event detection based on motion sensors versus force plates. *Journal of Neuroengineering and Rehabilitation*, 9, 10.

LIST OF PUBLICATIONS AND PAPERS PRESENTED

1. Tawfik Y Al-Nusairi, Nur Azah Hamzaid, Farahiyah Jasni, Hanie Nadia Shasmin (2020) Classification of Standing and Sitting Variations Based on In-Socket Piezoelectric Sensors in a Transfemoral Amputee, *Biomedical Engineering/ Biomedizinische Technik*, <https://doi.org/10.1515/bmt-2018-0249> (ISI-Indexed)
2. Farahiyah Jasni, Nur Azah Hamzaid, Nurhidayah Yusof, Tawfk Al-Nusairi, Hanie Nadia Shasmin, (2019) Feasibility of A Gait Phase Identification Tool for Transfemoral Amputees using Piezoelectric-Based In-Socket Sensory System, *IEEE Sensors Journal*, 19 (15): 6437-6444 (ISI-Indexed)